Supporting Supplementary Information

Donor-Acceptor Hetero[6]radialene-Based Three-Dimensional Covalent Organic Frameworks for Organic Pollutant Adsorption, Photocatalytic Degradation, and Hydrogen Production Activity

Jing Han Wang,[a] Ahmed E. Hassan,[b] Ahmed M. Elewa,[c] Ahmed F. M. EL-Mahdy[a*]

[a]Department of Materials and Optoelectronic Science, National Sun Yat-Sen University, Kaohsiung 80424, Taiwan.

[b]Department of Chemistry, Faculty of Science, Al-Azhar University, Nasr City 11884, Cairo, Egypt.

[c]Nuclear Chemistry Department, Hot Laboratories Center, Atomic Energy Authority, Cairo 13759, Egypt.

*To whom correspondence should be addressed

E-mail: ahmedelmahdy@mail.nsysu.edu.tw

Materials

Chemicals and solvents were acquired from commercial sources and used as obtained. Phloroglucinol (99%), bromine, potassium carbonate (K_2CO_3), nitrobenzene, 4-aminophenylboronic acid pinacol ester, acetic acid (CH_3COOH) and n-butanol were purchased from Sigma–Aldrich. Hexamethylenetetramine (99%) were obtained from SHOWA. Trifluoroacetic acid (99%) (TFA), pyrene, tetrakis(triphenylphosphine)palladium (0) Pd $(PPh_3)_4$, (4-aminophenyl) boronic acid, o-dichlorobenzene were obtained from Acros.

Hydrochloric acid (>37%) (HCl) were sourced from Fluka. Bis(pinacolato)diboron, [1,1′-bis(diphenylphosphino)ferrocene]dichloropalladium(II) (dffp), potassium acetate (AcOK), potassium hydroxide (KOH), chloroform ($CHCl_3$) were purchased from J. T. Baker.1,4-dioxane were obtained from Fisher Chemical.4-bromoaniline, phenanthrene-9,10-dione, benzoyl peroxide (BPO), potassium permanganate ($KMnO_4$), Lawesson's reagent were obtained from Alfa Aesar. Toluene, acetone was sourced from Echo Chemical Co. Tetrahydrofuran (THF) was purchased from HY Biocare Chem.

Characterizations

Fourier-transform infrared (FRIR) spectroscopy was recorded using a Bruker Tensor 27 FTIR spectrophotometer (USA) and the conventional KBr plate method; 32 scans were collected at a resolution of 4 cm^{-1}. Solid state nuclear magnetic resonance (SSNMR) spectroscopy was recorded using a Bruker Avance 400 NMR spectrometer and a Bruker magic-angle-spinning (MAS) probe (USA), running 32,000 scans. Thermogravimetric analysis (TGA) was performed using a TA Q-50 analyzer (USA) under a flow of N_2. The samples were sealed in a Pt cell and heated from 40 to 700 °C at a heating rate of 20 °C min^{-1} under N_2 at a flow rate of 50 mL min^{-1}. Nitrogen adsorption-desorption measurements were carried out using a BelSorp max instrument. Before measuring gas adsorption, the as-prepared samples (50 mg) were washed with anhydrous tetrahydrofurane for 24 hours using Soxhlet extraction. The solvent was filtered, and the samples were activated for 10 hours under pressure at 150 °C. The samples were then used for gas adsorption-desorption measurements at 77 K from 0 to 1 atm. Their specific surface areas were calculated using the Brunauer-Emmett-Teller (BET) methodology. The pore distributions were calculated from the sorption data using the quenched solid state density functional theory. Field-emission scanning electron microscopy (FE-SEM) was conducted using a JEOL JSM-7610F scanning electron microscope (USA) .

Samples were subjected to Pt sputtering for 100 s prior to observation. Transmission electron microscopy (TEM) was performed using a JEOL-2100 scanning electron microscope (USA), operated at 200 kV. Samples for UV–Vis and fluorescence spectroscopy were dissolved in suitable organic solvents and placed in a small quartz cell (0.2 × 1.0 × 4.5 cm^3). UV–Vis–NIR spectra were recorded at 25 °C using a Jasco V-570 spectrometer (Japan), with deionized water as the solvent. Photoluminescence (PL) was measured by HITACHI F-4500, using 150W Xe Lamp. The samples were mixed with DMF then placed in a small quartz cell and excited with 360 nm wavelength. Ultraviolet Photoelectron Spectroscopy (UPS) was carried out with ESCA003500, using the intensity of He I (21.2 eV). The samples were dropped on indium tin oxide (ITO) glasses. The photodegradation of dye and photocatalytic hydrogen evolution were performed using solar simulator of 7IS0503A, SOFN Instruments Co. Ltd. and the yield analysis of photocatalytic hydrogen evolution was obtained with Nexis GC-2030.

Synthetic procedures

Synthesis of 1,3,5-triformylphloroglucinol (TFP-3OHCHO)

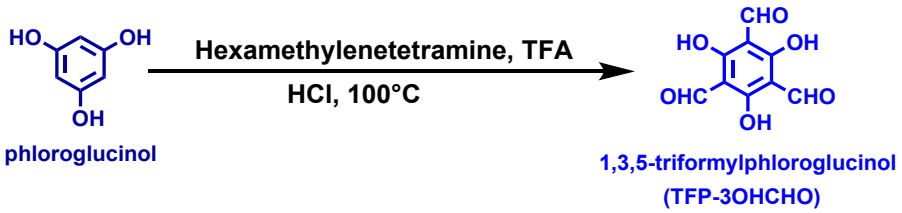

Scheme S1. Synthesis of 1,3,5-triformylphloroglucinol (TFP-3OHCHO).

Hexamethylenetetramine (5 g, 35.67 mmol) and phloroglucinol (2 g, 15.86 mmol) were added to a 250 mL two-neck round-bottomed flask with trifluoroacetic acid (30 mL) under N_2. The mixture solution was heated at 100 °C for 3 h. After adding 3 M hydrochloric acid (100 mL), the mixture was heated at 100 °C for 1 h. The reaction mixture was extracted three times with dichloromethane until it cooled down to room temperature. The extract was concentrated with rotatory evaporation and added to ethanol (50 mL). The product was filtered and washed

completely with ethanol (20 mL). The solid was dried under vacuum to obtain 1,3,5-triformylphloroglucinol as a pink powder.

Synthesis of 4,4',4'',4'''-pyrene-1,3,6,8-tetrayl) tetraaniline (PyTA-4NH$_2$)

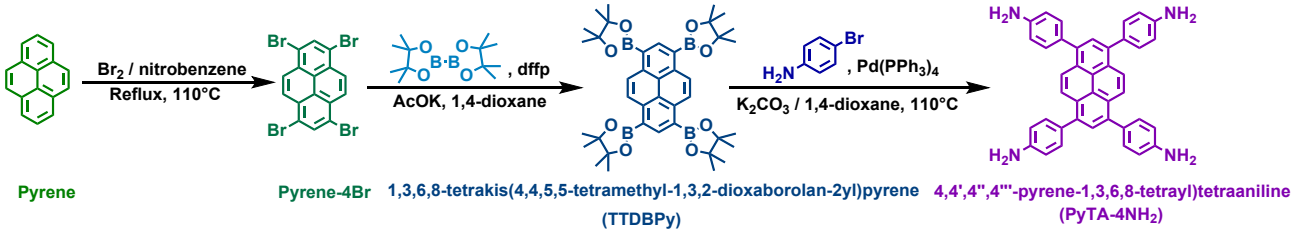

Scheme S2. Synthesis of 4,4',4'',4'''-pyrene-1,3,6,8-tetrayl) tetraaniline (PyTA-4NH$_2$)

1,3,6,8-tetrabromopyrene (Pyrene-4Br): In a 500 mL round-bottom flask, pyrene (5.0 g, 24 mmol) was dissolved in nitrobenzene (200 mL). Bromine (5.6 mL, 109 mmol) was added dropwise into the mixture by a dropping funnel. The reaction solution was refluxed at 110 °C for 15 h. The pale-yellow crystallites of 1,3,6,8-tetrabromopyrene were separated from the reaction solution after consuming bromine. The suspension was filtered and the solid was washed several times with ethanol. The pale-yellow product was dried under vacuum for 12 h to get a powder.

4,4',4'',4'''-pyrene-1,3,6,8-tetrayl) tetraaniline (PyTA-4NH$_2$): Pyrene-4Br (2.0 g, 3.8 mmol), bis (pinacolato) diboron (5.98 g, 23.56 mmol), [1,1'- Bis (diphenylphosphino) ferrocene] dichloro palladium (II) (241 mg, 0.033 mmol), and potassium acetate (2.33 g, 23.37 mmol) was put in a 100 mL round-bottom flask. After the mixture was evacuated under high pressure for 15 min, dioxane (40 mL) was added. The mixture refluxed for 48 h under an N_2 atmosphere flow. Until the reaction consumed pyrene-4Br, the mixture was cooled down to room temperature and then added to ice-water to yield a yellow precipitate. The precipitate was filtered and washed with several times with water. The solid was purified by flash column chromatography with THF and hexane as the eluent. The isolate product was

finally recrystallized with methanol to acquire 1,3,6,8- tetrakis (4,4,5,5-tetramethyl-1,3,2-dioxaborolan-2-yl) pyrene (TTDBPy) as yellow crystals.

TTDBPy (1.0 g, 1.41 mmol), 4-bromoaniline (1.95 g, 11.33 mmol), tetrakis (triphenylphosphine) palladium (0) (80.88 mg, 0.07 mmol), and potassium carbonate (1.95 g, 14.1 mmol) were added to a 100 mL round-bottom flask. After the solid was evacuated under high pressure for 15 min, dioxane (40 mL) and water (7 mL) were added. The mixture was heated at 100 °C for 48 h under N_2. Until the reaction-consumed TTDBPy, the mixture was cooled down to room temperature and then put in ice-water to yield a yellow-greenish precipitate. The solid was filtered and washed several times with water/ methanol/dichloromethane. 4,4',4",4"'-pyrene-1,3,6,8-tetrayl) tetraaniline (PyTA-4NH_2) without further purification was used as the final product.

Synthesis of 4,4',4'',4'''-([9,9'-bifluorenylidene]-3,3',6,6'-tetrayl)tetraaniline (BFTB-4NH_2)

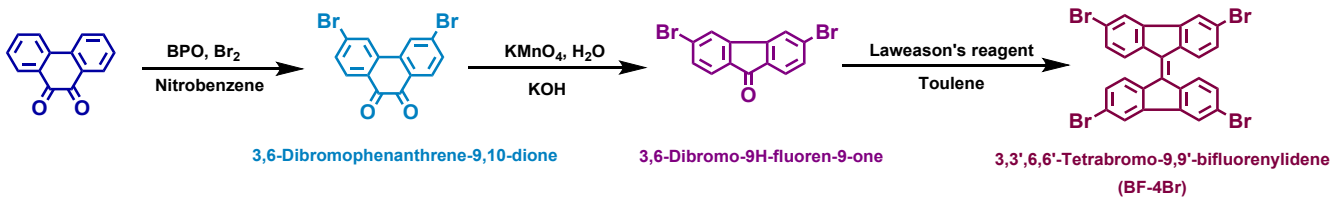

Scheme S3. Synthesis of 3,3',6,6'-Tetrabromo-9,9'-bifluorenylidene (BF-4Br)

3,6-Dibromophenanthrene-9,10-dione: At room temperature, phenanthrene-9,10-dione (5 g, 24 mmol) and dibenzoyl peroxide (0.2 g, 0.83 mmol) were weighed into a 250 mL two-neck round-bottomed flask with nitrobenzene (30 mL). Bromine (1.4 g, 8.7 mmol) was added dropwise into the mixture and heated at 110 °C. Then, bromine (6.9 g, 43.3 mmol) was added drop by drop to the mixture for two hours. The mixture was cooled and diluted with ethanol (30 mL). The solid was filtered and washed several times with ethanol. The isolated product was dried at 60 °C to obtain 3,6-dibromophenanthrene-9,10-dione as an orange powder.

3,6-Dibromo-9H-fluoren-9-one: In a 250 mL two-neck round-bottomed flask, potassium hydroxide (8.15 g, 0.18 mol) was dissolved in water (60 mL). 3,6-dibromophenanthrene-9,10-dione (5 g, 13.6 mmol) was weighed to the solution and heated at 130 °C for two hours. Potassium permanganate (11.43 g, 72.3 mmol) was added, and the mixture continued to be heated at 130 °C. After heating for two hours, the reaction mixture was cooled down to room temperature and neutralized to pH = 7 with diluted sulfuric acid. Sodium bisulfite was added slowly until a light-yellow solid had completely precipitated. The solid was filtered and washed several times with water. The product was dried at 60 °C to obtain 3,6-dibromo-9H-fluoren-9-one as a light-yellow powder.

Synthesis of 3,3',6,6'-Tetrabromo-9,9'-bifluorenylidene (BF-4Br): 3,6-dibromo-9H-fluoren-9-one (1 g, 2.96 mmol) and Lawesson's reagent (0.6 g, 1.483 mmol) were charged with dry toluene (40 mL) and then refluxed at 110 °C for 20 h. After cooling to room temperature, the precipitate was separated by filtration. After heating in acetone for 10 min, the mixture was filtered. The product was dried at 60 °C to get BF-4Br as an orange powder.

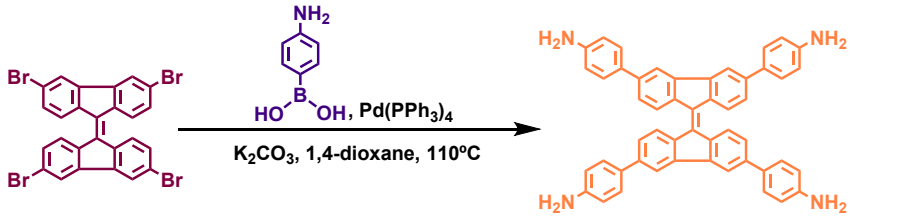

Scheme S4. Synthesis of 4,4',4'',4'''-([9,9'-bifluorenylidene]-3,3',6,6'-tetrayl) tetraaniline ($BFTB\text{-}4NH_2$)

4,4',4'',4'''-([9,9'-bifluorenylidene]-3,3',6,6'-tetrayl)tetraaniline ($BFTB\text{-}4NH_2$): BF-4Br (1 g, 1.55 mmol), 4-aminophenylboronic acid pinacol ester (2.70 g, 12.3 mmol), tetrakis (triphenylphosphine) palladium (0) (90 mg, 0.077 mmol), and potassium carbonate (2.15 g, 15.55 mmol) were added in a 100 mL round-bottom flask. After the solid was evacuated

under high pressure for 15 min, dioxane (50 mL) and water (10 mL) were poured. The mixture was heated at 100 °C for 48 h under N_2. Until BF-4Br was consumed, the reaction mixture was cooled to room temperature and poured into ice water to get a white precipitate. The precipitate was filtered and washed several times with water/methanol. The product was dried at 60 °C to obtain BFTB-4NH_2 as a blue powder.

Spectral Profiles of monomers

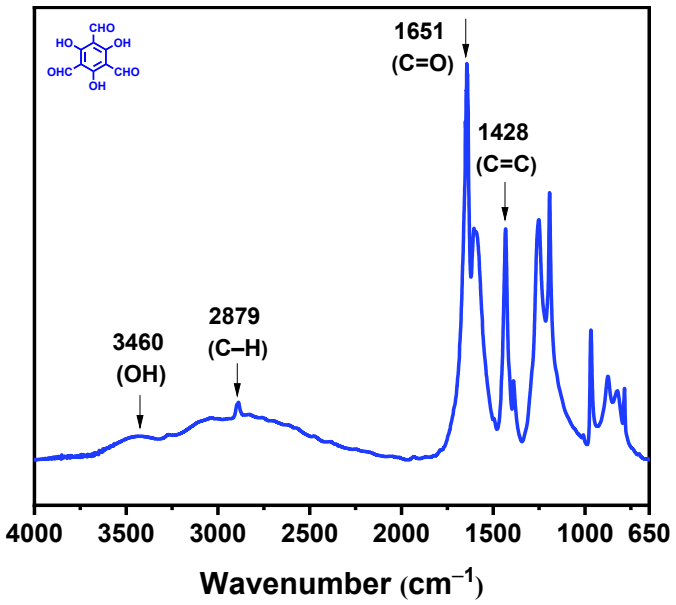

Figure S1. IR spectrum of 1,3,5-triformylphloroglucinol (TFP-3OHCHO).

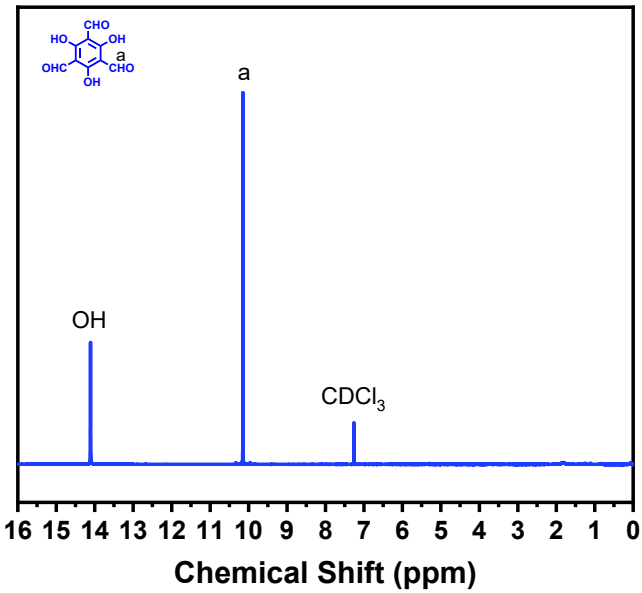

Figure S2. ^{1}H-NMR spectrum of 1,3,5-triformylphloroglucinol (TFP-3OHCHO).

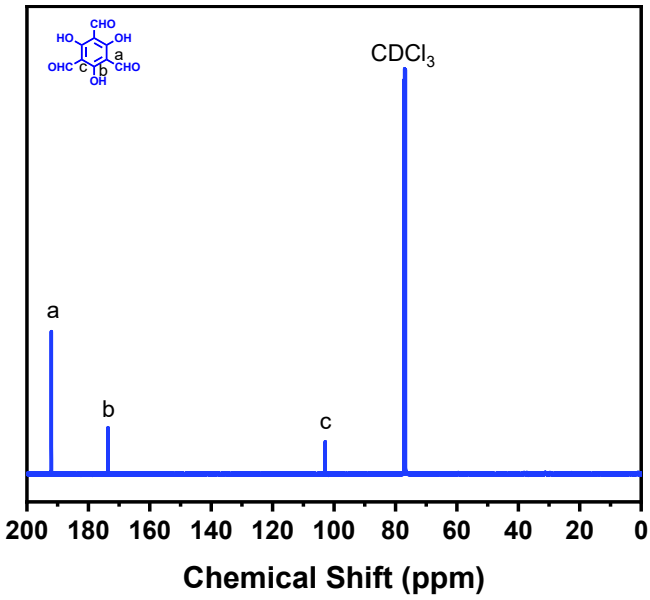

Figure S3. ^{13}C-NMR spectrum of 1,3,5-triformylphloroglucinol (TFP-3OHCHO).

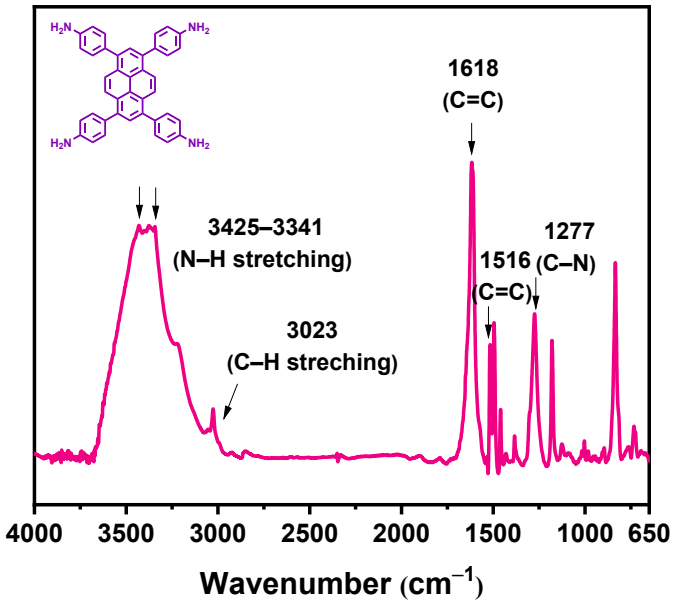

Figure S4. IR spectrum of 4,4',4",4"'-pyrene-1,3,6,8-tetrayl) tetraaniline (PyTA-4NH$_2$).

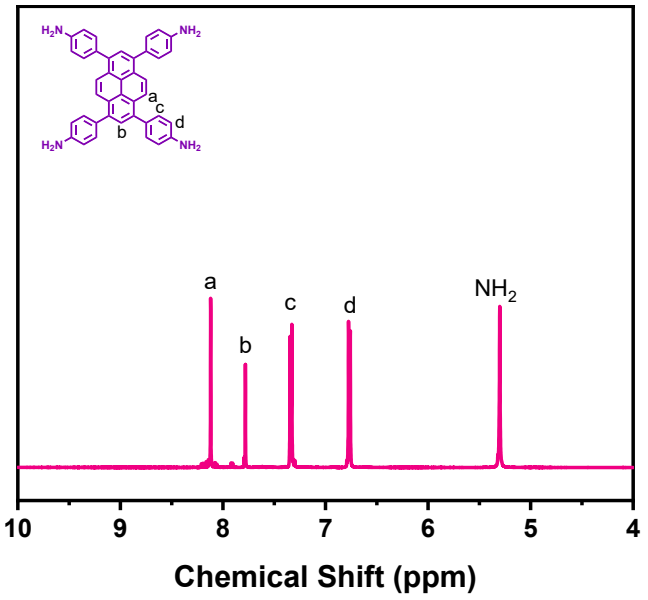

Figure S5. ^{1}H-NMR spectrum of 4,4',4",4"'-pyrene-1,3,6,8-tetrayl) tetraaniline (PyTA-4NH_2).

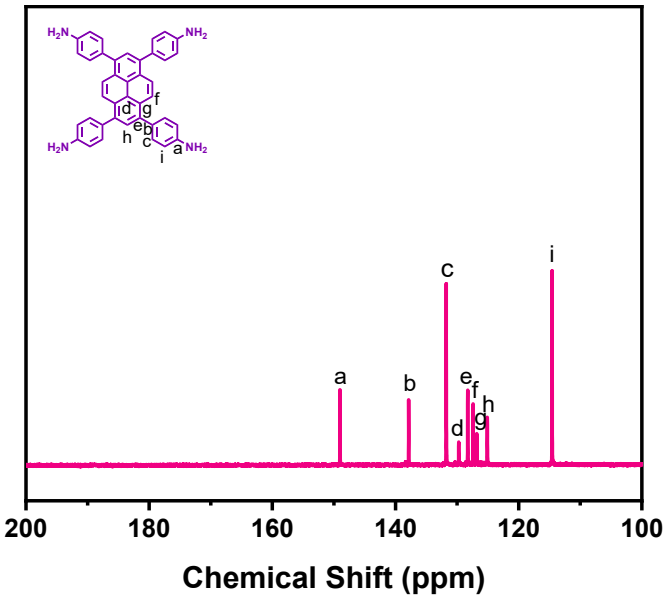

Figure S6. ^{13}C-NMR spectrum of 4,4',4",4"'-pyrene-1,3,6,8-tetrayl) tetraaniline (PyTA-4NH_2).

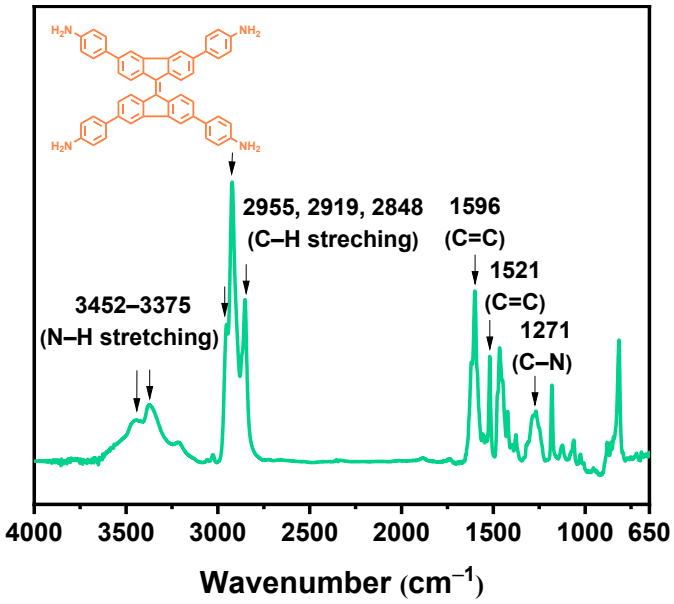

Figure S7. IR spectrum of 4,4',4",4"'-([9,9'-bifluorenylidene]-3,3',6,6'-tetrayl) tetraaniline (BFTB-4NH_2).

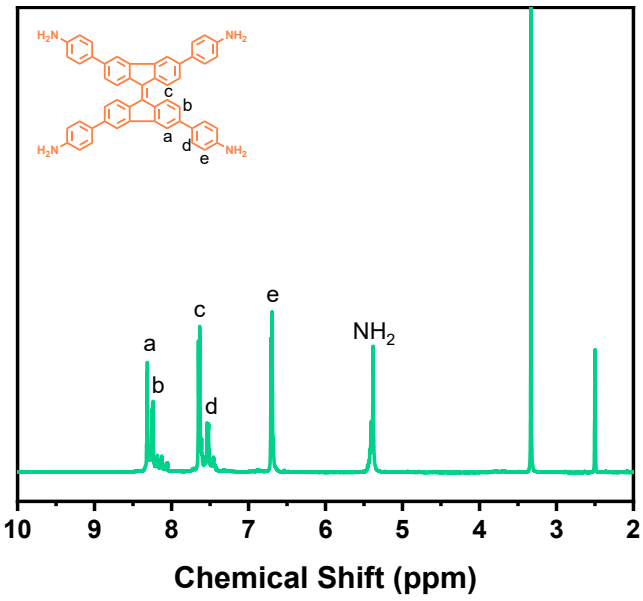

Figure S8. ^{1}H-NMR spectrum of 4,4',4",4"'-([9,9'-bifluorenylidene]-3,3',6,6'-tetrayl) tetraaniline (BFTB-4NH_2).

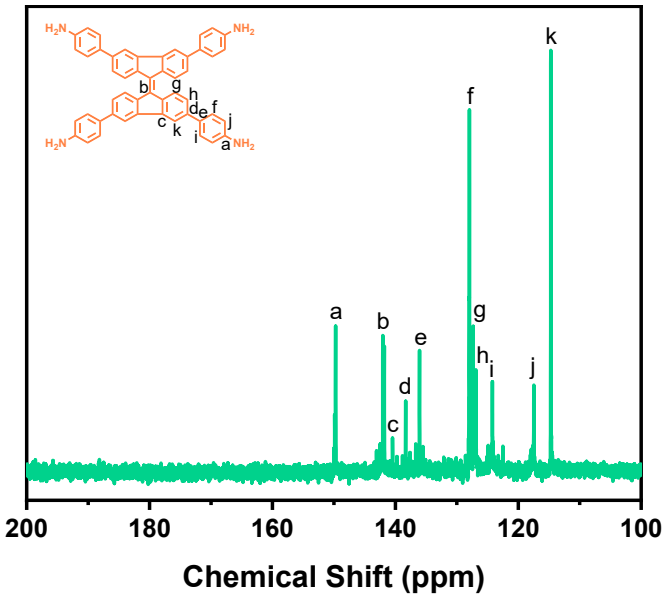

Figure S9. ^{13}C-NMR spectrum of 4,4',4'',4'''-([9,9'-bifluorenylidene]-3,3',6,6'-tetrayl) tetraaniline (BFTB-4NH_2).

PXRD data

Table S1. Fractional atomic coordinates for the unit cell of TFP-Py 3D COF.

Sample Name: TFP-Py 3D							
Space Group: P 1							
a = 36.9148 Å, b = 19.2861 Å, c = 39.9578 Å, α = 76.58°, β = 76.58°, γ= 91.34°							
Atom	*x/a*	*y/b*	*z/c*	Atom	*x/a*	*y/b*	*z/c*
N	0.16708	0.32151	-0.03233	C	0.39202	0.58572	0.2896
N	0.15772	0.69363	0.22678	C	0.37693	0.64375	0.06636
N	0.27913	0.58587	0.13839	C	0.33975	0.6436	0.02008
O	0.1135	0.49538	0.17584	C	0.43144	0.58769	0.35333
O	0.21465	0.64804	-0.16782	C	0.45364	0.52812	0.36915
O	0.22619	0.42122	-0.20195	C	0.48922	0.5306	0.48103
C	0.0388	0.06664	0.32557	C	0.50338	0.59409	0.55424
C	0.02183	0.12903	0.36263	C	0.48274	0.65627	0.49489
C	0.07564	0.06796	0.19313	C	0.44676	0.651	0.40853
C	0.10017	0.13322	0.11109	C	0.5583	0.53312	0.73298
C	0.13357	0.13168	0.26332	C	0.53731	0.59295	0.69481
C	0.15629	0.19303	0.20227	C	0.01844	0.00079	0.4296
C	0.14575	0.2572	-0.00641	H	0.03579	0.18051	0.29249
C	0.11344	0.25809	-0.17362	H	0.14145	0.08356	0.43959
C	0.09121	0.19628	-0.12038	H	0.18115	0.19163	0.33277
C	0.14973	0.38672	-0.01308	H	0.10548	0.30665	-0.3452
C	0.16752	0.44822	-0.00259	H	0.06657	0.19825	-0.25285
C	0.20755	0.46119	-0.07242	H	0.19457	0.31633	0.01127
C	0.22499	0.52602	-0.00816	H	0.12023	0.38473	0.02127
C	0.20218	0.5883	-0.0274	H	0.11418	0.61377	0.26615
C	0.16315	0.57645	0.08921	H	0.18529	0.69817	0.26854
C	0.14594	0.50622	0.09015	H	0.02528	0.82105	0.51402
C	0.14288	0.6263	0.19165	H	0.1762	0.80608	0.47154
C	0.13566	0.75326	0.24305	H	0.13969	0.9096	0.49918
C	0.03508	0.93633	0.40158	H	0.05485	0.82172	0.01071
C	0.07222	0.93811	0.27238	H	0.09024	0.71812	-0.00277
C	0.01421	0.87221	0.5121	H	0.88094	-0.00591	0.94533
C	0.14951	0.80921	0.37294	H	0.27451	0.47693	0.07471
C	0.12868	0.86834	0.38632	H	0.26633	0.63389	0.13137
C	0.0936	0.87331	0.26489	H	0.31437	0.48192	0.54912
C	0.08062	0.81828	0.12233	H	0.37899	0.48414	0.655
C	0.10101	0.75847	0.11632	H	0.39384	0.68929	-0.07288
C	0.90887	-0.00415	0.83795	H	0.32856	0.68852	-0.15314
C	0.26011	0.52577	0.06429	H	0.43039	0.69749	0.38019
C	0.3171	0.58496	0.18875	H	0.58367	0.53493	0.85158
C	0.33176	0.52699	0.41197	H	0.54763	0.6378	0.78531
C	0.3687	0.52814	0.46904				

Table S2. Fractional atomic coordinates for the unit cell of TFP-Py 3D COF..

Sample Name: TFP-BF 3D							
Space Group: P 1							
a = 46.6438 Å, b = 25.6726 Å, c = 31.070 Å, α = 90.00°, β = 90.00°, γ= 93.10°							
Atom	*x/a*	*y/b*	*z/c*	Atom	*x/a*	*y/b*	*z/c*
N	0.16314	0.39117	0.32921	C	0.09268	0.93683	0.08068
N	0.1651	0.70095	0.13844	C	0.07163	0.97988	0.09812
N	0.26975	0.50312	0.04708	C	0.10369	0.83457	0.10968
N	0.85954	0.36079	0.0859	C	0.09182	0.77926	0.14849
N	0.86051	0.67063	0.27228	C	0.1119	0.73551	0.15596
N	0.75239	0.46526	-0.04789	C	0.14442	0.74596	0.12475
O	0.1242	0.54479	0.35156	C	0.15654	0.80097	0.08317
O	0.2187	0.64561	0.09453	C	0.1363	0.84508	0.07614
O	0.21714	0.45191	0.26302	C	0.25171	0.55147	0.06562
O	0.80664	0.60941	0.17637	C	0.47409	0.59257	-0.51863
O	0.89991	0.5175	0.295	C	0.50305	0.56974	-0.55556
O	0.80594	0.41519	0.04201	C	0.52932	0.60366	-0.65706
C	0.01205	0.05911	0.17987	C	0.5261	0.66116	-0.70167
C	0.03919	0.10055	0.22158	C	0.49669	0.68398	-0.65362
C	0.07109	0.0936	0.28216	C	0.47018	0.64944	-0.56396
C	0.0918	0.1409	0.31717	C	0.49931	0.5083	-0.51171
C	0.0806	0.19512	0.29832	C	0.46519	0.49796	-0.44451
C	0.0483	0.20124	0.24962	C	0.45067	0.54809	-0.44577
C	0.02847	0.15374	0.21431	C	0.41881	0.55145	-0.36759
C	0.1022	0.24538	0.32167	C	0.40096	0.50193	-0.28314
C	0.1349	0.24126	0.32916	C	0.41598	0.45094	-0.27255
C	0.15494	0.28943	0.33584	C	0.44812	0.44887	-0.34857
C	0.14253	0.34218	0.33573	C	0.5218	0.47053	-0.52186
C	0.10992	0.34636	0.33168	C	0.5561	0.48041	-0.46553
C	0.09001	0.29848	0.32455	C	0.51783	0.40932	-0.57899
C	0.15113	0.44561	0.32977	C	0.57043	0.43015	-0.48287
C	0.16875	0.4932	0.28909	C	0.6024	0.42612	-0.41707
C	0.20325	0.49481	0.23413	C	0.62066	0.47501	-0.32905
C	0.22092	0.5487	0.14869	C	0.60592	0.52618	-0.30271
C	0.2041	0.60122	0.15004	C	0.57361	0.52894	-0.36636
C	0.16969	0.59983	0.21652	C	0.49129	0.37602	-0.67983
C	0.15244	0.54588	0.29031	C	0.49428	0.31874	-0.73844
C	0.15282	0.64529	0.20768	C	0.52371	0.29553	-0.70496
C	0.03969	0.96654	0.15532	C	0.55047	0.32949	-0.61635
C	0.02929	0.91117	0.1745	C	0.54678	0.38616	-0.55709
C	0.04946	0.86778	0.15719	C	0.65475	0.47268	-0.25754
C	0.0818	0.88042	0.11394	C	0.36701	0.5031	-0.19937

Continuous (**Table S2**)

Atom	*x/a*	*y/b*	*z/c*	Atom	*x/a*	*y/b*	*z/c*
C	0.66913	0.42142	-0.25633	C	0.92164	0.81622	0.28732
C	0.7013	0.4193	-0.18776	C	0.88894	0.82047	0.28608
C	0.71956	0.46833	-0.1194	C	0.86882	0.77239	0.28513
C	0.70538	0.51965	-0.12066	C	0.88115	0.71957	0.28592
C	0.67325	0.52176	-0.18892	C	0.91376	0.71527	0.29039
C	0.352	0.55373	-0.1866	C	0.93375	0.76306	0.29088
C	0.31991	0.55434	-0.10657	C	0.77228	0.51371	0.02927
C	0.30246	0.50419	-0.03823	H	0.08012	0.04987	0.30278
C	0.31726	0.4538	-0.05094	H	0.11795	0.13573	0.36132
C	0.34926	0.45321	-0.13059	H	0.03877	0.24466	0.23965
C	0.95285	0.08165	0.07786	H	0.1453	0.19851	0.32982
C	0.98464	0.09495	0.14579	H	0.18146	0.28571	0.34139
C	0.995	0.1503	0.16855	H	0.09956	0.38913	0.33423
C	0.9749	0.19372	0.14391	H	0.06349	0.30218	0.32097
C	0.94268	0.18112	0.08951	H	0.18894	0.38731	0.32359
C	0.93186	0.12473	0.05305	H	0.12489	0.45065	0.36661
C	0.92086	0.22703	0.0772	H	0.12641	0.64128	0.25795
C	0.93273	0.28237	0.1147	H	0.19068	0.70934	0.0952
C	0.91269	0.32619	0.11533	H	0.03972	0.82273	0.17801
C	0.88021	0.31576	0.07842	H	0.11877	0.94789	0.03921
C	0.86809	0.26072	0.03796	H	0.08067	1.02519	0.06568
C	0.8883	0.21656	0.03773	H	0.06545	0.76972	0.17436
C	0.8717	0.4166	0.15236	H	0.10192	0.69073	0.18767
C	0.85465	0.46187	0.15946	H	0.18294	0.81003	0.05491
C	0.87169	0.51606	0.23245	H	0.14626	0.88984	0.04304
C	0.85519	0.56855	0.22899	H	0.26441	0.59358	0.00668
C	0.82075	0.56651	0.16773	H	0.25835	0.46121	0.10096
C	0.8032	0.51255	0.09511	H	0.55291	0.58456	-0.70236
C	0.82021	0.45992	0.09477	H	0.54741	0.68969	-0.77733
C	0.87261	0.61626	0.27341	H	0.49432	0.73078	-0.68755
C	1.01222	1.00237	0.17986	H	0.44633	0.6681	-0.53031
C	0.98499	0.96094	0.21194	H	0.40776	0.59362	-0.37288
C	0.95296	0.96792	0.26127	H	0.40192	0.41057	-0.20124
C	0.93215	0.92064	0.28838	H	0.45991	0.40746	-0.33148
C	0.94335	0.86641	0.27272	H	0.61327	0.38386	-0.435
C	0.97576	0.86025	0.23568	H	0.62034	0.56606	-0.22871
C	0.99571	0.90773	0.20824	H	0.56204	0.57042	-0.33679

Continuous (**Table S2**)

Atom	*x/a*	*y/b*	*z/c*	Atom	*x/a*	*y/b*	*z/c*
H	0.46766	0.39545	-0.71338	H	0.92266	0.37097	0.14603
H	0.47276	0.2907	-0.81369	H	0.84173	0.2517	0.00506
H	0.52591	0.24888	-0.74993	H	0.87834	0.17178	0.00539
H	0.57434	0.31056	-0.59469	H	0.83399	0.35243	0.04
H	0.65455	0.38105	-0.31162	H	0.89786	0.42528	0.20493
H	0.71272	0.37746	-0.18749	H	0.89905	0.61519	0.31589
H	0.72009	0.55989	-0.06578	H	0.83479	0.67528	0.2607
H	0.66182	0.56359	-0.18924	H	0.94391	1.01165	0.27921
H	0.36598	0.59474	-0.24169	H	0.90592	0.92585	0.32344
H	0.30794	0.59563	-0.09691	H	0.98528	0.8168	0.22859
H	0.3032	0.41286	0.00391	H	0.8786	0.86327	0.28583
H	0.36123	0.41193	-0.14029	H	0.84231	0.77623	0.2837
H	0.94412	0.03621	0.04308	H	0.92407	0.67245	0.29364
H	0.98461	0.23876	0.16778	H	0.96026	0.75923	0.2942
H	0.90587	0.1137	0.00293	H	0.76321	0.42424	-0.05121
H	0.95907	0.29186	0.14514	H	0.76203	0.55657	0.03752

Spectral Profiles of COFs

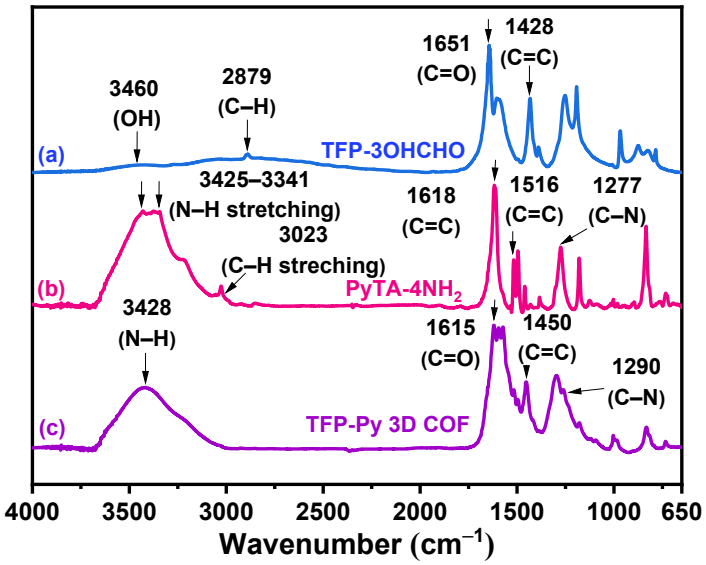

Figure S10. IR spectrum of (a) TFP-3OHCHO, (b) PyTA-4NH_2 and (c) TFP-Py 3D COF.

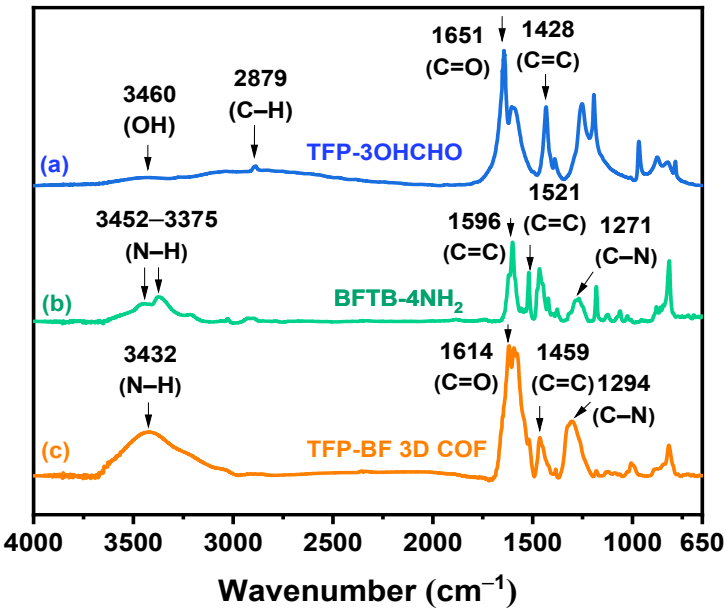

Figure S11. IR spectrum of (a) TFP-3OHCHO, (b) BFTB-4NH_2 and (c) TFP-BF 3D COF.

Hydrogen bonding formation

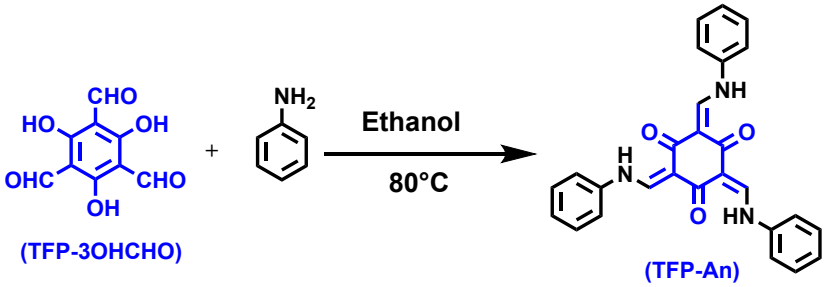

Scheme S5. Synthesis of the model compound TFP-An (J. H. Chong, M. Sauer, B. O. Patrick, M. J. MacLachlan, Org. Lett. 2003, 5, 21, 3823–3826).

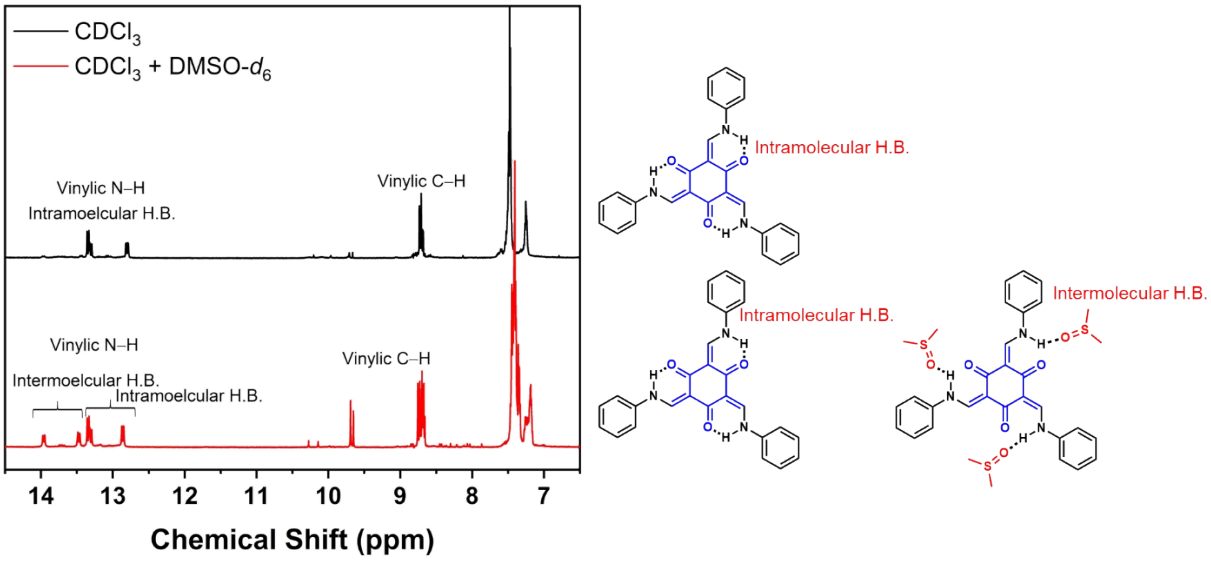

Figure S12. Variation in the chemical shift of the vinylic N–H for the compound TFP-An in 100% $CDCl_3$ (black curve) and 30% of DMSO-d_6 in $CDCl_3$ (red curve).

Thermogravimetric analysis

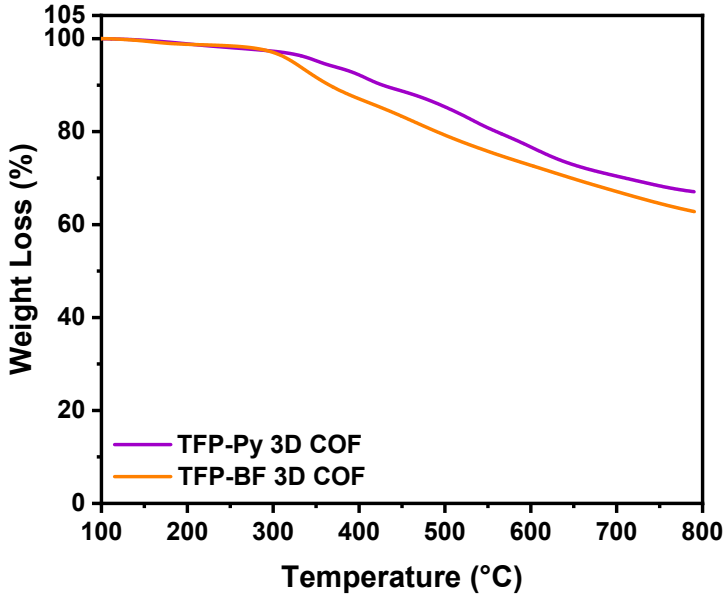

Figure S13. TGA analysis of TFP-Py and TFP-BF 3D COFs.

Table S3. Values of T_{d10}, and Char yield of TFP-Py and TFP-BF 3D COFs.

COFs	T_{d10} (°C)	Char yield (%)
TFP-Py 3D COF	427.52	67.07
TFP-BF 3D COF	365.16	62.77

BET parameter of COF

Table S4. BET parameters of TFP-Py and TFP-BF 3D COFs.

COFs	S_{BET} ($m^2 g^{-1}$)	Pore Volume ($cm^3 g^{-1}$)	Pore Size (nm)
TFP-Py 3D COF	731	0.94	0.97/1.73
TFP-BF 3D COF	447	0.99	1.01/1.82

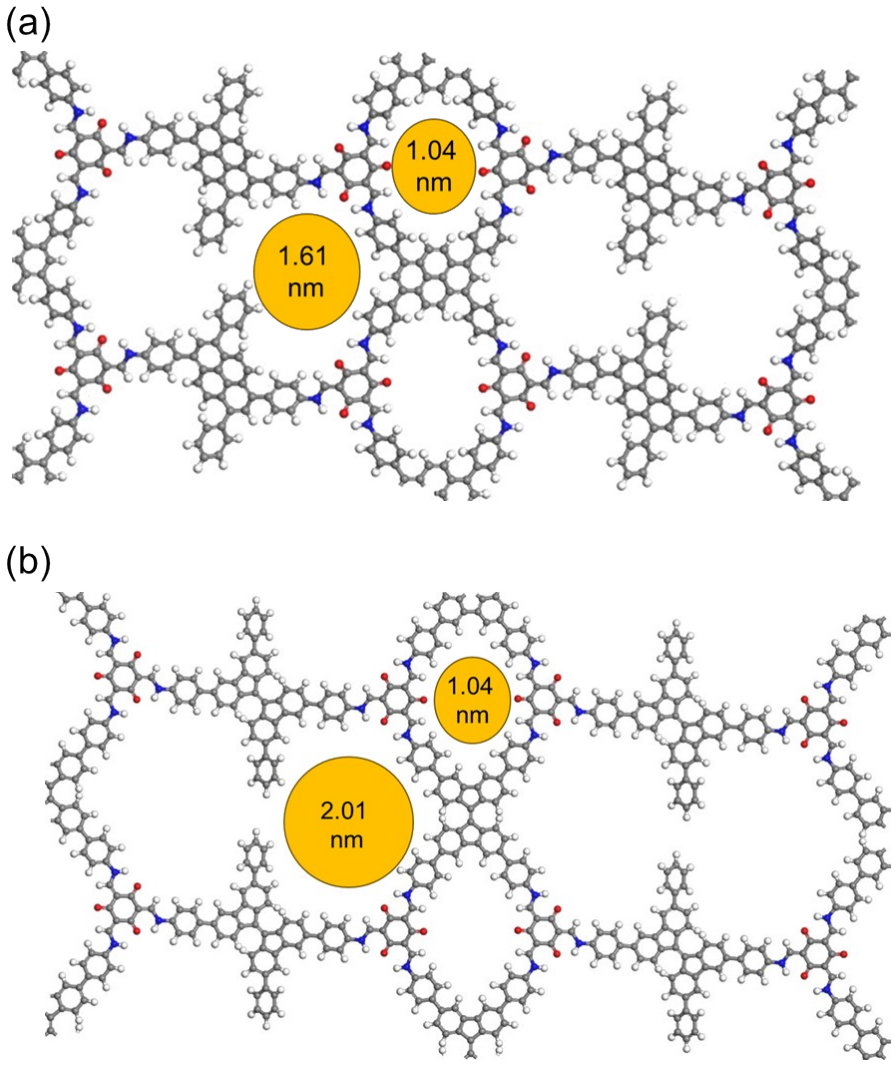

Figure S14. Theoretical pore diameters as obtained from the crystal structure model of the (a) TFP-Py and (b) TFP-BF 3D COFs.

X-ray photoelectron spectroscopy analysis

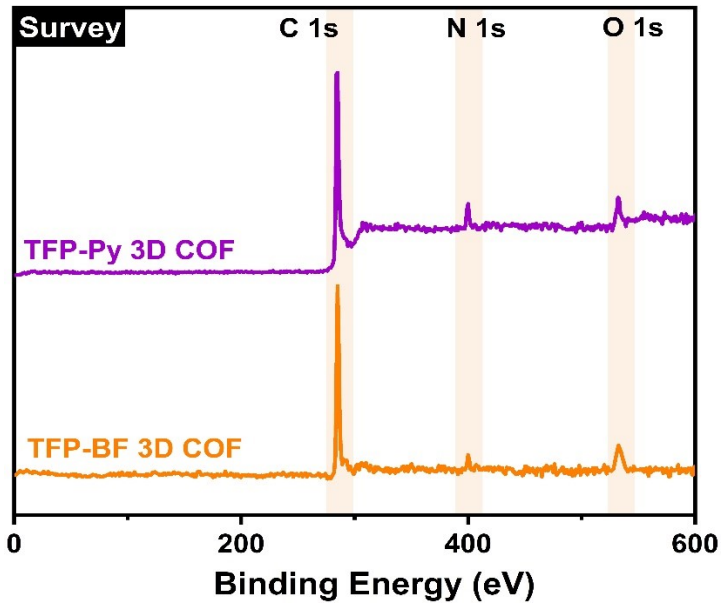

Figure S15. XPS survey spectra of TFP-Py and TFP-BF 3D COFs.

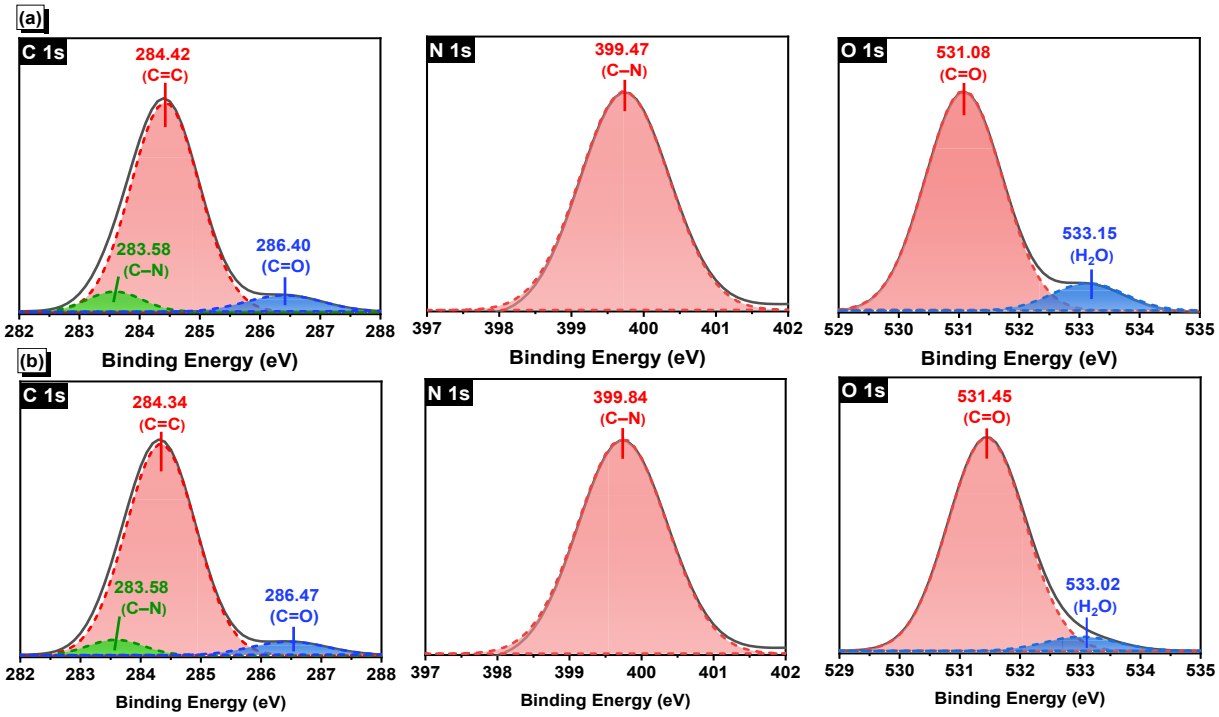

Figure S16. Fitting curves of C 1s, N 1s, and O 1s XPS spectra of (a) TFP-Py and (b) TFP-BF 3D COFs.

Table S5. XPS fitting position of TFP-Py and TFP-BF 3D COFs.

COFs	C species (eV)			N species (eV)	O species (eV)	
	C–N	C=C	C=O	C–N	C=O	H_2O
TFP-Py 3D COF	283.58	284.42	286.40	399.47	531.08	533.15
TFP-BF 3D COF	283.58	284.34	286.47	399.84	531.45	533.02

Table S6. XPS fitting ratio of TFP-Py and TFP-BF 3D COFs.

COFs	C species (eV)			N species (eV)	O species (eV)	
	C–N	C=C	C=O	C–N	C=O	H_2O
TFP-Py 3D COF	6.69	85.67	7.64	100.00	89.46	10.54
TFP-BF 3D COF	5.12	88.65	6.23	100.00	94.12	5.88

Electronic band levels

For optical band gaps for TFP-Py COF and TFP-BF COF, the Tauc plot was performed according to the Kubelka–Munk function.[S1-S5] The following equation is used to calculate optical band gap using absorption spectra:

$$\alpha h\nu = A(h\nu - Eg)^{n/2}$$

Where α is the optical absorption coefficient, h is the Planck constant, ν is the light frequency, E_g is the optical band gap, and A is the a cinstant depending on electron-hole mobility. The value of n is 1. Then, The E_g of the samples could well be determined from a plot of $(\alpha h\nu)^{1/2}$ versus energy (hν), and its value can be derived from the intercept of the tangent to the X axis.

The energy levels of the HOMO were measured using a photoelectron spectrometer (model AC-2). The energy levels of the LUMOs were calculated by subtracting the Eg from the HOMO energy levels.

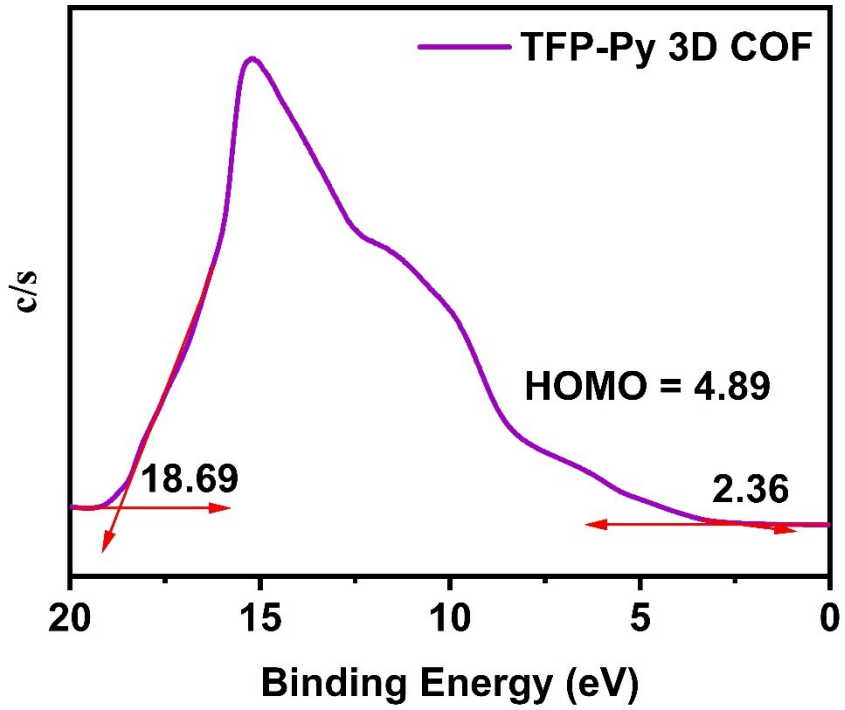

Figure S17. Ultraviolet photoemission spectroscopy (UPS) measurement of TFP-Py 3D COF.

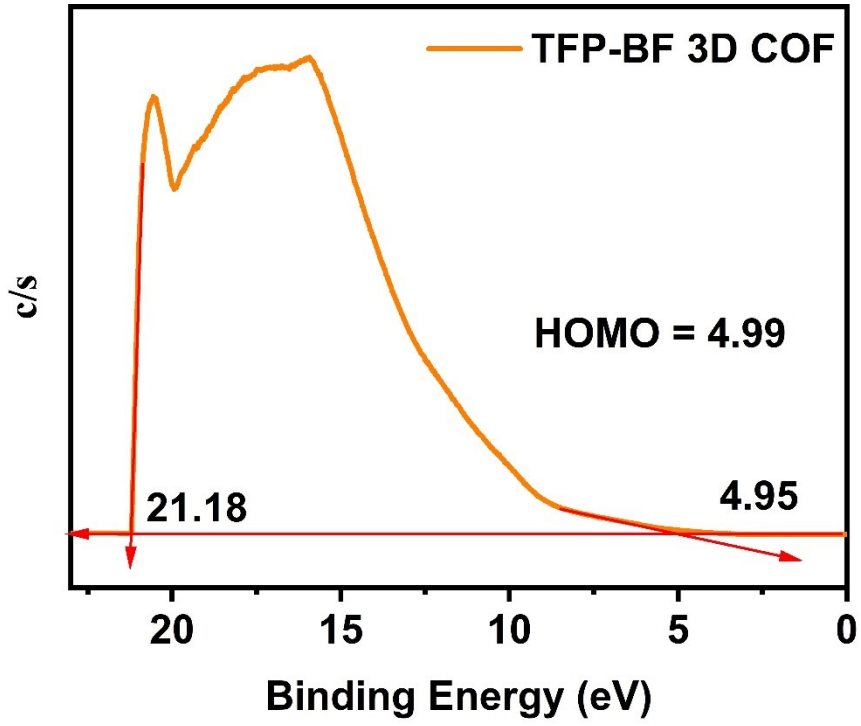

Figure S18. Ultraviolet photoemission spectroscopy (UPS) measurement of TFP-BF 3D COF.

Table S7. Absorption maxima and energy levels of TFP-Py and TFP-BF 3D COFs.

COFs	λ_{max} (nm)[a]	E_g (nm)[b]	HOMO (eV)[c]	LUMO (eV)[d]
TFP-Py 3D COF	523	1.95	−4.89	−2.94
TFP-BF 3D COF	607	1.80	−4.99	−3.19

[a] Absorption was determined in the solid state using reflectance mode; [b] Determined by the onset of UV-vis absorption; [c] Calculated from the photoelectron spectrometer; [d] Calculated from LUMO = HOMO[d] – Eg.

Time-resolved fluorescence lifetime decays

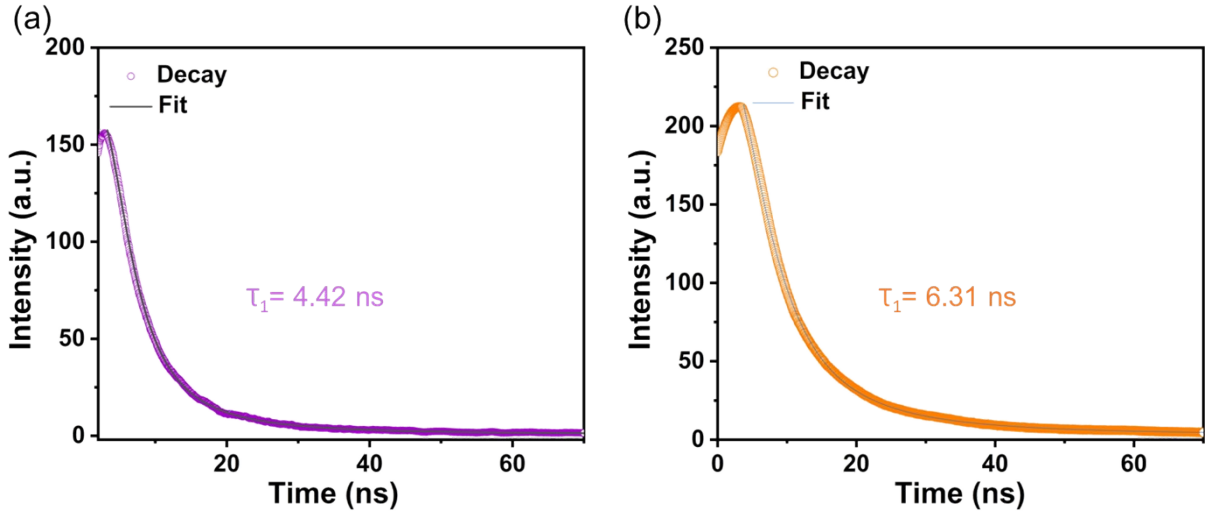

Figure S19. Time-resolved fluorescence lifetime decay spectra of (a) TFP-Py and (b) TFP-BF 3D COFs.

Photocurrent Measurement

The photocurrent response measurements were performed on a Zahner Zennium 6273E workstation equipped with visible-light irradiation with a conventional three-electrode cell including a Pt wire counter electrode, Ag/AgCl as reference electrode (3 M NaCl) and an indium tin oxide (ITO) glass as working electrode. About 5 mg of TFP-Py COF and TFP-BF COF were dispersed into an acetonitrile solution (1 mL) with 30 µL Nifion and sonicate for 30 min to obtain a slurry mixture. After that, 200 µL of as-prepared slurry was spread onto ITO

glass with an active area of 6.875 cm^2. Here, 0.5 M Na_2SO_4 aqueous solution was prepared as electrolyte. 0.8 V constant potential was applied with the 30 s light on-off after a certain time interval to record the photo and dark current. A 300 W Xe lamp with a visible-light band-pass filter (λ > 450 nm) was employed as the excitation light source.

Electrochemical impedance spectroscopy

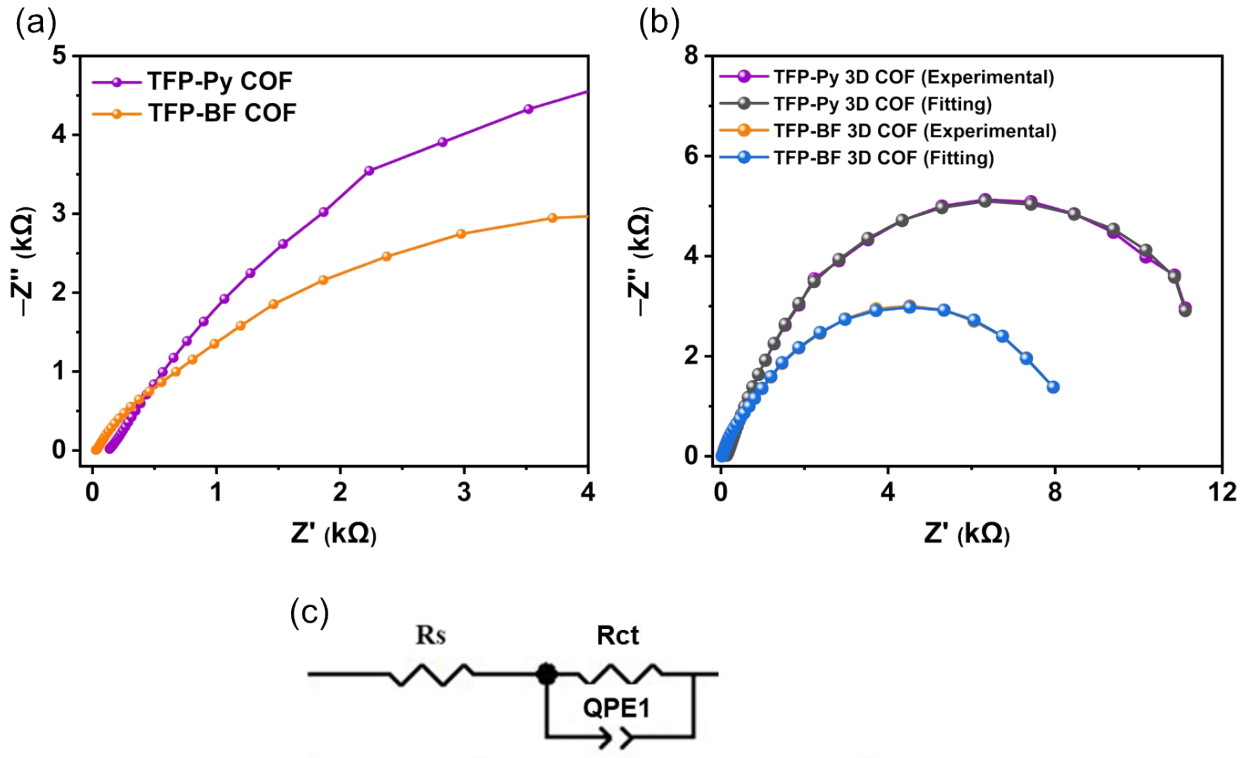

Figure S20. (a) The Nyquist plots of the TFP-Py and TFP-BF 3D COFs at the high-frequency region, under visible light irradiation (λ > 400 nm) (b) The fitted Nyquist plots using (c) the equivalent circuit of TFP-Py and TFP-BF 3D COFs.

Table S8. The fitting values of Nyquist plots of TFP-Py and TFP-BF 3D COFs.

3D COF	Rs (Ω)	Rct (Ω)
TFP-Py	138	14315
TFP-BF	28	9062

Dye adsorption Experiments

The performance of the TFP-Py COF and TFP-BF COF for dye removal from water was demonstrated using RhB organic dye. In this experiment, a weight of 4 mg of TFP-Py COF and TFP-BF COF was added to an aqueous solution of RhB (10 mL, 18 mg L^{-1}) in a glass vial with stirring for (0, 5, 10, 20, 30, and 60 min) at a rate of 800 rpm, at 25 °C and pH = 7. Centrifugation (6000 rpm, 10 min) was then carried out to isolate the supernatant, then the UV–Vis spectrum of the isolated supernatant was recorded.

Different concentrations of dye solution (from 12.5 to 200 mg L^{-1}) were used in order to obtain adsorption isothermal curves. At every experiment, a specific amount of TFP-Py COF and TFP-BF COF (4 mg) was added to the previous prepared RhB aqueous solutions (10 mL) in a glass vial with stirring at a rate of 800 rpm for a period of 24 h, at 25 °C and pH = 7. The clear dye solution was separated from mother liquor using centrifugation and then, its UV–Vis spectrum was measured. The equilibrium adsorption of dye per unit mass of the adsorbent, Q_e (mg g^{-1}),[S9] was estimated as follows:

$$Q_e = (C_0 - C_e) \times V \times m^{-1}$$

Where C_0 (mg L^{-1}) is the initial dye concentration in the liquid phase, C_e (mg L^{-1}) is the equilibrium dye concentration in the liquid phase, V (L) is volume of dye solution, and m (mg) is the mass of COF.

The adsorption isotherms were fitted using the Langmuir isothermal model (linear form) which presented as follows:

$$\frac{C_e}{Q_e} = \frac{1}{K_L Q_m} + \frac{C_e}{Q_m}$$

where K_L (L mg^{-1}) is the Langmuir constant; and Q_m (mg g^{-1}) is the maximum equilibrium adsorption of dye per unit mass of the adsorbent.

Table S9. Fitted parameters of Langmuir isothermal model for adsorption of TFP-Py and TFP-BF 3D COFs.

COFs	Q_m (mg g^{-1})	K_L (L mg^{-1})	R_L^2
TFP-Py 3D COF	840	0.305	0.9995
TFP-BF 3D COF	520	0.712	0.9994

Mechanism of Adsorption

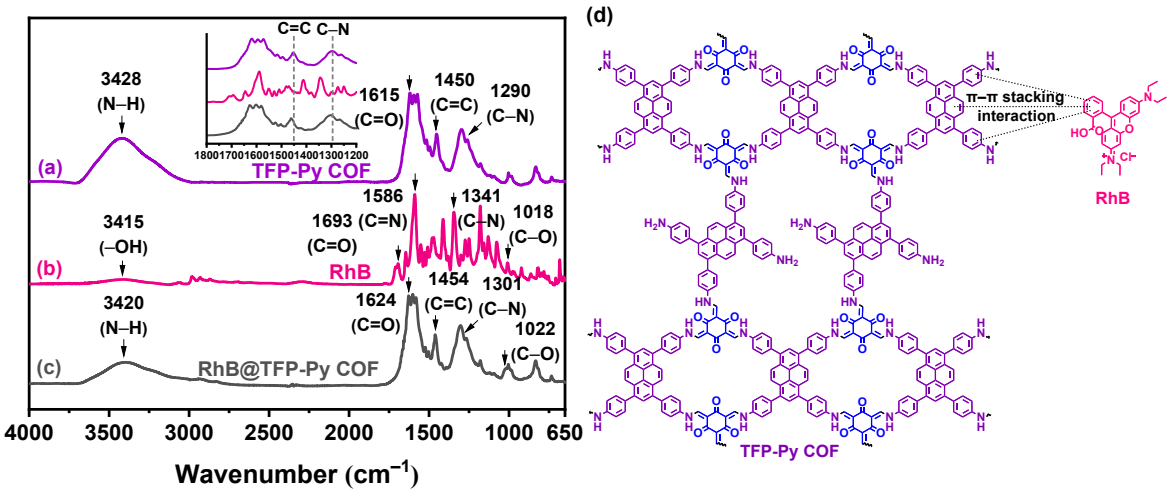

Figure S21. FTIR spectra of (a) TFP-Py 3D COF, (b) rhodamine B (RhB), and (c) TFP-Py 3D COF after adsorbed rhodamine B. (d) Adsorption mechanism of rhodamine B on TFP-Py 3D COF.

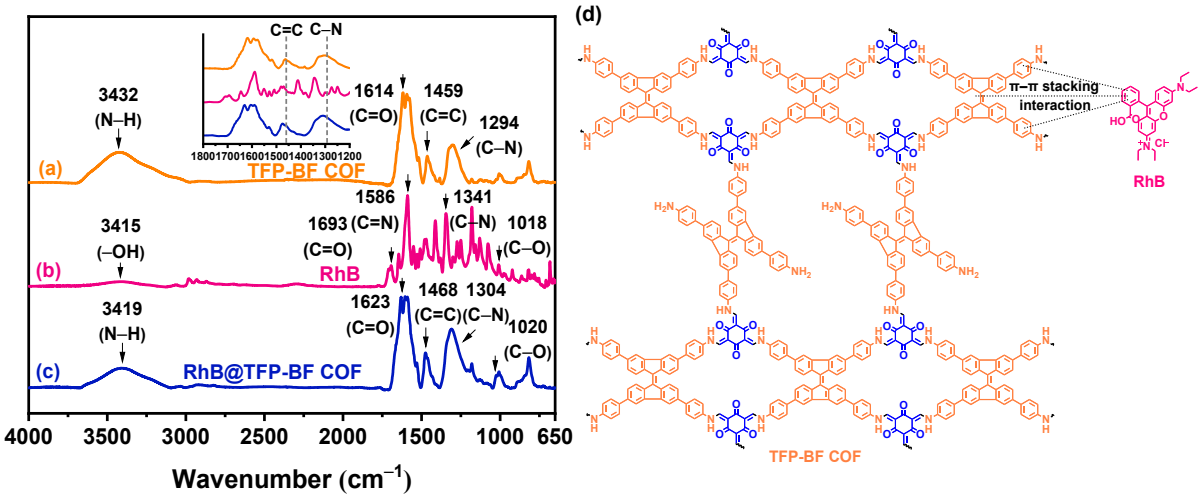

Figure S22. FTIR spectra of (a) TFP-BF 3D COF, (b) rhodamine B (RhB), and (c) TFP-BF 3D COF after absorbed rhodamine B. (d) Adsorption mechanism of rhodamine B on TFP-BF 3D COF.

Table S10. Maximum adsorption capacities of RhB on the TFP-Py and TFP-BF 3D COFs, compared with those of other reported materials.

Adsorbent	Dye	Q_m (mg g^{-1})	BET (m^2 g^{-1})	Amount/dye conc.	Ref.
CMP-YA	RhB	535	1410	0.2 mg mL^{-1}/25 mg L^{-1}	*Macromolecules*, 2017, *50*, 4993–5003
Py-BF-CMP	RhB	1905	1306	0.2 mg mL^{-1}/25 mg L^{-1}	Macromolecules, 2018, 51, 3443–3449
TPE-BF-CMP	RhB	1024	777	0.2 mg mL^{-1}/25 mg L^{-1}	Macromolecules, 2018, 51, 3443–3449
TPA-BF-CMP	RhB	926	590	0.2 mg mL^{-1}/25 mg L^{-1}	*Macromolecules,* 2018, *51*, 3443–3449
Ttba-TPDA-COF	RhB	833	726	0.5 mg mL^{-1}/20-800 mg L^{-1}	Ind. Eng. Chem. Res., 2020, 59, 8315–8322
CuP-DMNDA-COF/Fe	RhB	378-429	273	0.25 mg mL^{-1}/16 mg L^{-1}	New J. Chem., 2017, 41, 6145–6151
BIPE-BIPE	RhB	352	918	0.4 mg mL^{-1}/25 mg L^{-1}	New J. Chem. 2021, 45, 21834–21843
BIPE-Py	RhB	1027	1400	0.4 mg ml^{-1}/25 mg L^{-1}	New J. Chem. 2021, 45, 21834–21843
BIPE-TPT	RhB	739	903	0.4 mg mL^{-1}/25 mg L^{-1}	New J. Chem. 2021, 45, 21834–21843
TFP-Py 3D COF	RhB	840	731	0.4 mg mL^{-1}/18 mg L^{-1}	**This work**
TFP-BF 3D COF	RhB	520	447	0.4 mg mL^{-1}/18 mg L^{-1}	**This work**

Photodegradation Experiments

The blank experiment without adding TFP-Py COF and TFP-BF COF were conducted with 56 mL of RhB solution (10 mg L^{-1}) and irradiated for 180 min. The distance between the liquid level and the filter is fixed at 8 cm.

In a typical Photodegradation experiment, a weight of 7 mg of TFP-Py COF and TFP-BF COF were added to an aqueous solution of RhB (56 mL, 10 mg L^{-1}) in a glass in a 100 mL sandwich beaker and magnetically stirred with the rate of 600 rpm for 60 min in the dark for reaching the saturation of adsorption of dye. The entire mixture was kept at room temperature by using circulating water. The entire mixture was irradiated during the photocatalytic experiment for 180 min for TFP-Py COF and TFP-BF COF. An aliquot of the reaction mixture (3 mL) was taken by a pipette every 30 min to monitor the degradation process, for which the catalyst was removed through centrifugation (4000 rpm, 2 min). Then, the UV–Vis spectrum of the isolated supernatant was recorded. The degradation efficiency (%) was calculated from the equation listed below:

$$Degradation\ efficiency\ (\%) = \frac{C_0 - C_e}{C_0} \times 100\ \%$$

Where C_0 (mg L^{-1}) is the initial dye concentration in the liquid phase and C_e (mg L^{-1}) is the equilibrium dye concentration in the liquid phase at t = 0 and t minutes of photocatalytic reaction.

For reusability of TFP-Py COF and TFP-BF COF for organic RhB dye degradation, the solutions were filtered to recover the TFP-Py COF and TFP-BF COF catalysts, and to guarantee that the adsorbed dyes were removed, the catalysts were washed with a significant amount of water and ethanol. The recovered catalysts were then activated under a vacuum at 80 °C for 1 night. Each cycle experiment was carried out under identical conditions to verify the correctness of the results.

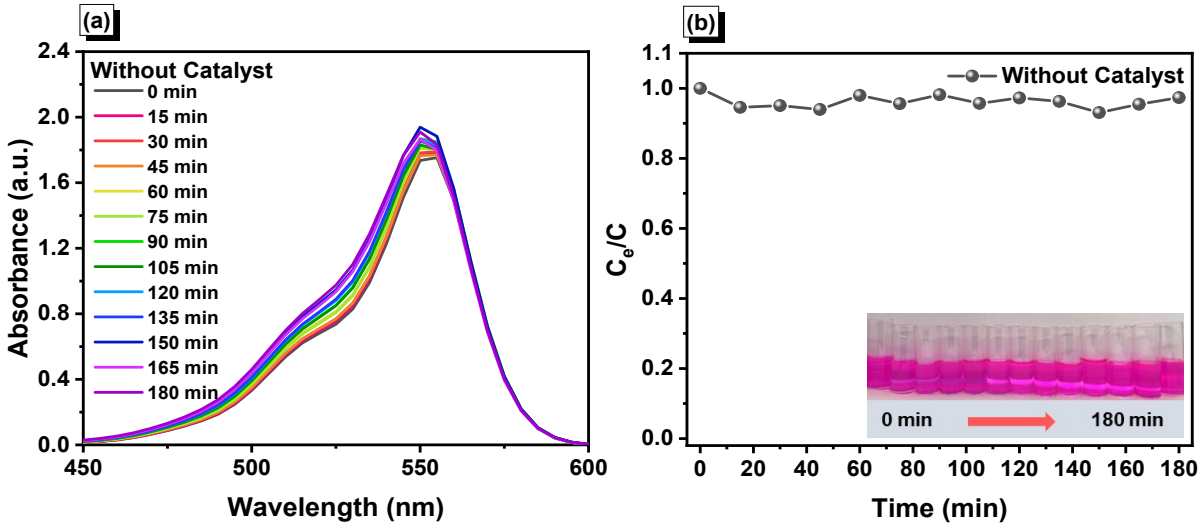

Figure S23. (a) UV-Vis spectra and (b) Photocatalytic efficacy of the control experiment of RhB upon UV and visible light irradiation without catalyst.

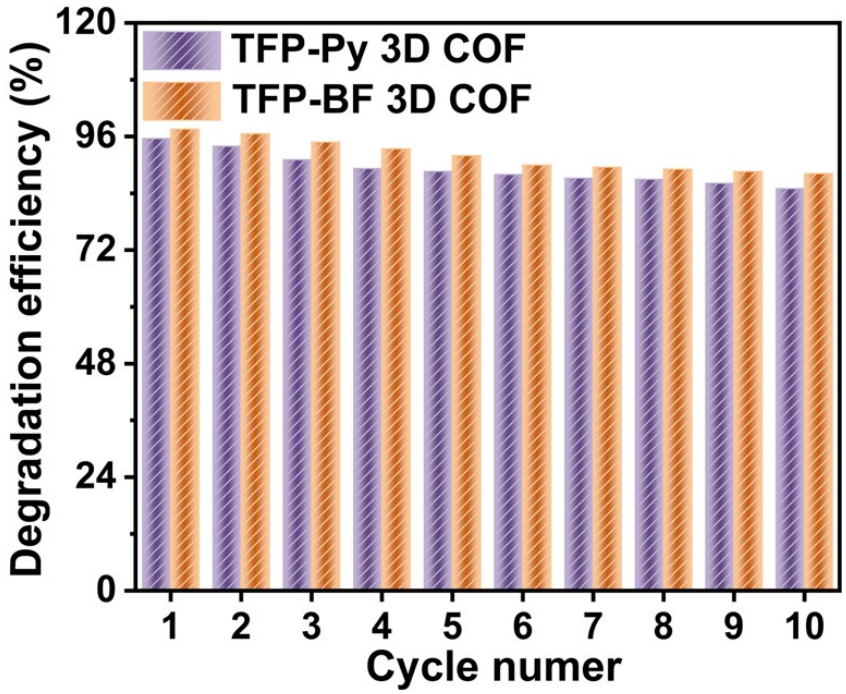

Figure S24. Reusability of TFP-Py and TFP-BF 3D COFs for RhB photodegradation within 165 min.

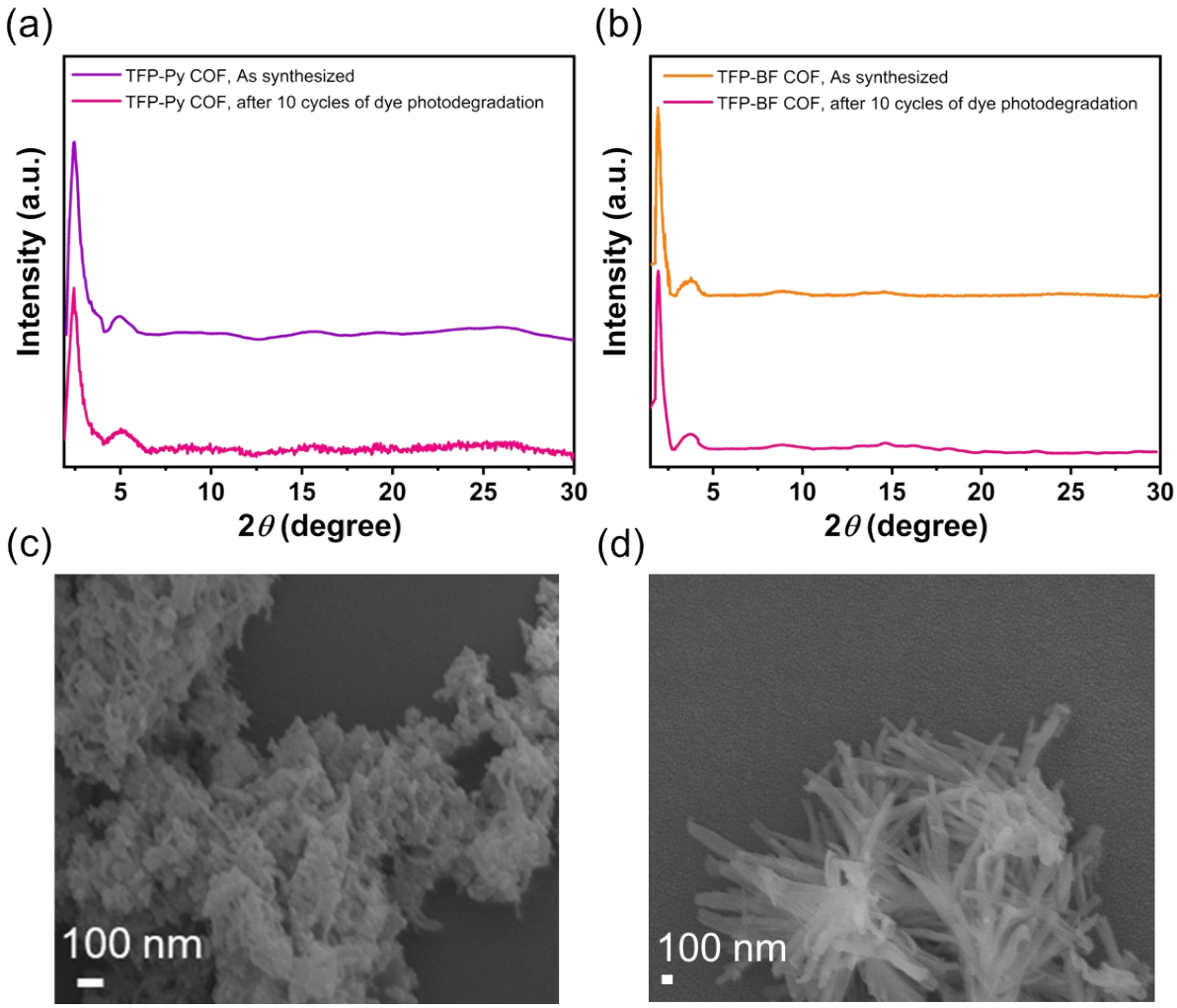

Figure S25. PXRD patterns of (a) TFP-Py and (b) TFP-BF 3D COFs before and after 10 cycles of dye photodegradation. FE-SEM images of (c) TFP-Py and (d) TFP-BF 3D COFs after 10 cycles of dye photodegradation.

Mechanism of Photodegradation

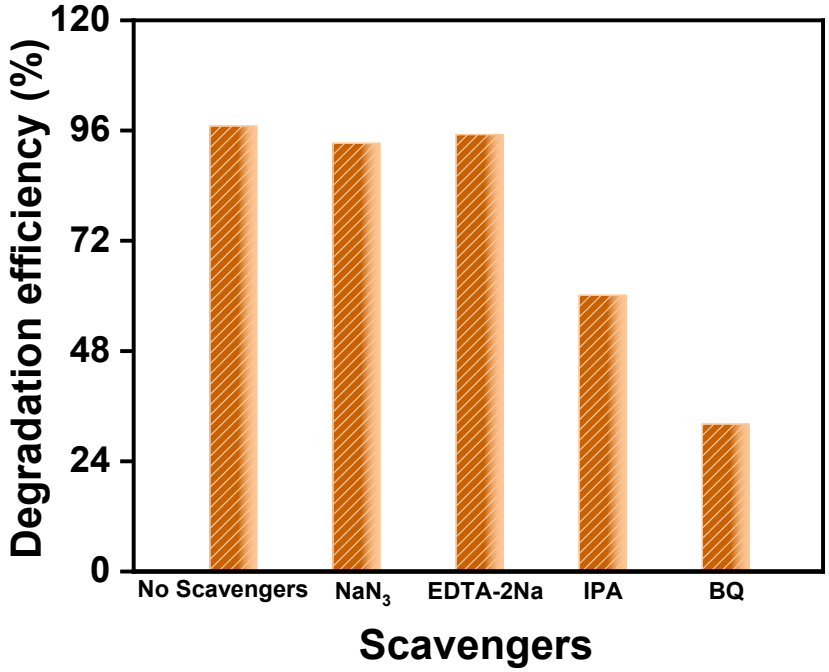

Figure S26. Effect of different scavengers, NaN_3, EDTA-2Na, IPA, and BQ on the photocatalytic degradation of RhB (10 mg L^{-1}) by TFP-BF 3D COF for 165 min.

Table S11. Photodegradation performance of RhB on the TFP-Py COF and TFP-BF COF, compared with those of other reported materials.

Catalyst	Catalyst amount (mg)	Dye RhB solution	Degradation time (min)	Degradation efficiency (%)	Ref.
COF/g-C_3N_4	20	10 mg L^{-1}, 50 mL	20	~100	*Dalton Trans.,* 2019, *48*, 14989–95
Au@COF	10	10 mg L^{-1}, 100 mL	30	97.3	
POP-1	20	4.8 mg L^{-1}, 10 mL	180	93.3	*J. Mater. Chem. A,* 2020, *8*, 7003-34.
Py-POP	10	4.8 mg L^{-1}, 10 mL	80	~100	*Microporous Mesoporous Mater.,* 2020, *292*, 109774
TP-COP	100	10 mg L^{-1}, 100 mL	160	95	*Cryst. Growth Des., 2019, 19, 2525-30*
COF-JLU19	5	10 mg L^{-1}, 100 mL	6	~100	*Chinese J. Catal., 2021, 42, 2010-19*
Py-BF-CMP	10	75 mg L^{-1}, 50 mL	90	<90.00	*Macromolecules, 2018, 51, 3443-49*
TPE-BF-CMP	10	55 mg L^{-1}, 50 mL	90	~90.00	*Macromolecules, 2018, 51, 3443-49*
TPA-BF-CMP	10	40 mg L^{-1}, 50 mL	90	~90.00	*Macromolecules, 2018, 51, 3443-49*
Py-CMP-1	6	20 mg L^{-1}, 60 mL	90	16.20	*Polym. Chem., 2022, 13, 5300-08*
Py-CMP-2	6	20 mg L^{-1}, 60 mL	90	95.77	*Polym. Chem., 2022, 13, 5300-08*
TFP-Py 3D COF	7	10 mg L^{-1}, 56 mL	195	95.90	**This work**
TFP-BF 3D COF	7	10 mg L^{-1}, 56 mL	150	96.60%	**This work**

Photocatalytic Hydrogen Evolution Experiments

Photocatalytic H_2 evolution test

The photocatalytic experiments were performed in a 35-mL Pyrex reactor. The reactor was sealed using a rubber septum. In a typical photocatalytic reaction, a COF (2 mg) was dispersed in a mixture of water/DMF (2/1, 10 mL) with 1 M AA as the SED and adjusted the pH to 4.0 using 1M KOH. The suspension was purged with Ar for 5 min to remove dissolved air. A 350-W Xe lamp was used as the light source. The light intensity of the Xe lamp was similar to that of the visible light region of standard 1 sun irradiation, as verified using a solar cell. Samples of H_2 were removed with a gas-tight syringe and injected in a Nexis GC-2030 gas chromatograph with Ar as the carrier gas. The H_2 was detected using a thermal conductivity detector, with reference to standard H_2 gases of known concentrations.

Quantum efficiency measurements

For the AQY experiments, a catalyst solution was prepared by dispersing COF (1 mg) in a mixture of water/DMF (2/1, 10 mL) with 1 M AA. The suspension was illuminated with a 300-W Xe lamp while applying bandpass filters (420, 460, and 500 nm). The formation of H_2 was quantified using a Nexis gas chromatograph (GC-2030) operated under isothermal conditions, employing a semi capillary column equipped with a thermal conductivity detector. The AQY was calculated as follows:

AQY = [(number of evolved H_2 molecules × 2)/number of incident photons] × 100%

$$AQY = \frac{2 \times number\ of\ evolved\ H2\ molecules}{number\ of\ incident\ photons} \times 100\%$$

$$AQY = \frac{N_e}{N_p} \times 100\% = \frac{2 \times M \times N_A}{\frac{E_{total}}{E_{photon}}} \times 100\%$$

$$= \frac{2M \times N_A}{\frac{S \times P \times t}{h \times \frac{c}{\lambda}}} \times 100\% = \frac{2 \times M \times N_A \times h \times c}{S \times P \times t \times \lambda} \times 100\%$$

where M is the amount of H_2 (mol), N_A is Avogadro's constant (6.022×10^{23} mol^{-1}), h is Planck's constant (6.626×10^{-34} J·s), c is the speed of light (3×10^8 m s^{-1}), S is the irradiation area (cm^2), P is the intensity of irradiation light (W cm^{-2}), t is the photoreaction time (s), and λ is the wavelength of the monochromatic light (m).

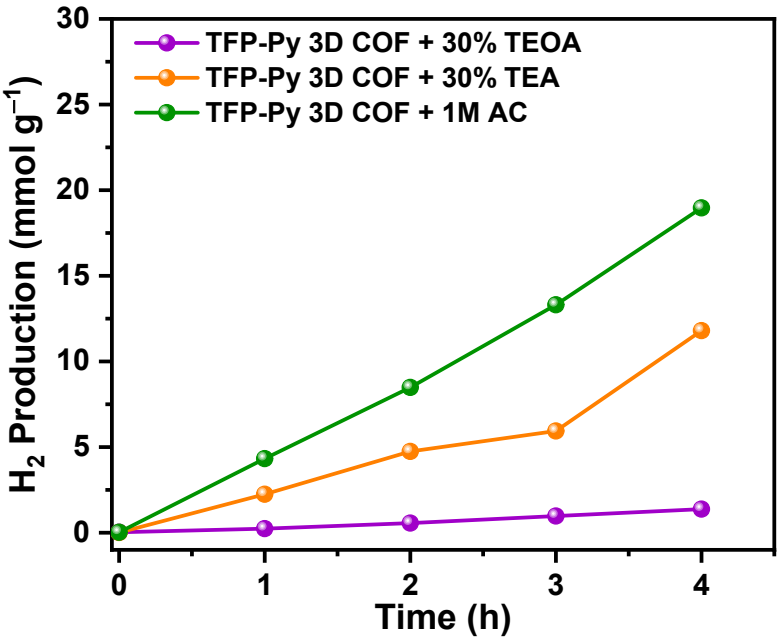

Figure S27. HERs of TFP-Py 3D COF under UV-Vis light with different sacrificial hole-scavengers, the dosage of each COF is 2 mg.

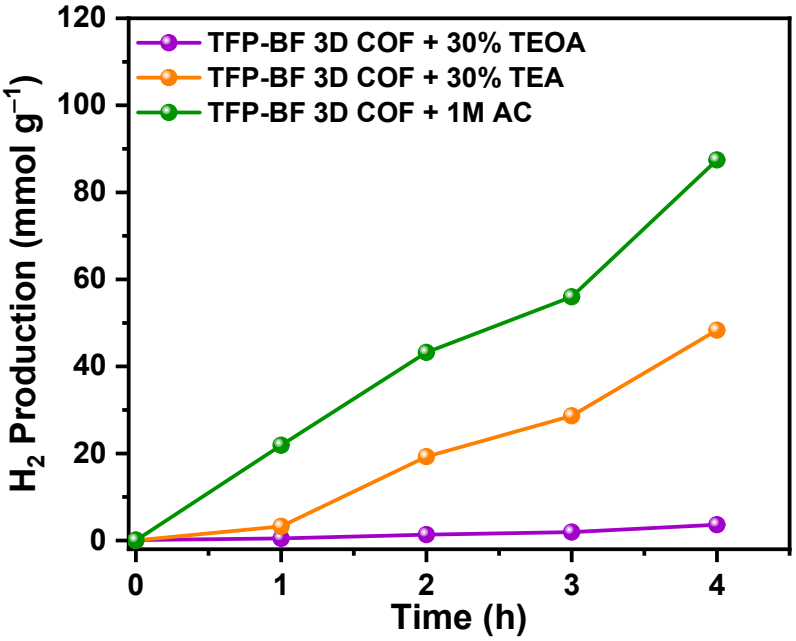

Figure S28. HERs of TFP-BF 3D COF under UV-Vis light with different sacrificial hole-scavengers, the dosage of each COF is 2 mg.

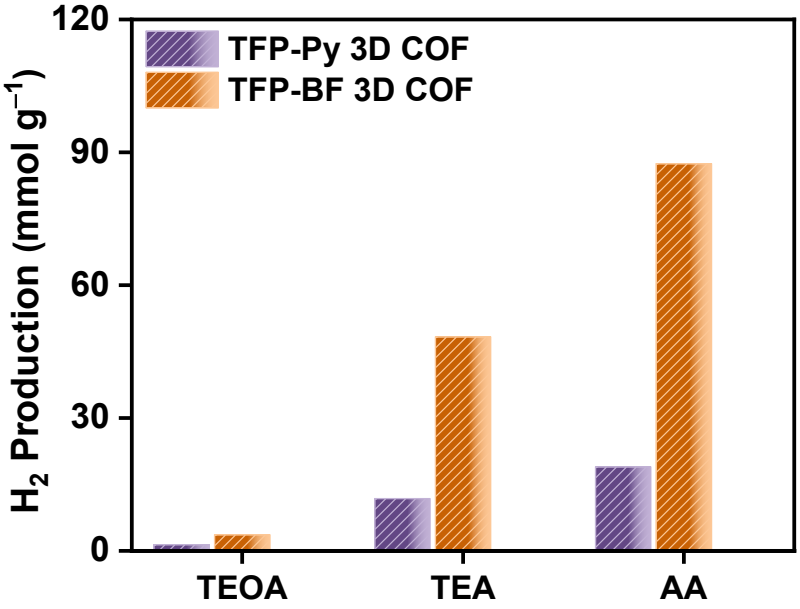

Figures 29. Comparison of HERs of TFP-Py and TFP-BF 3D COFs under UV-Vis light with different sacrificial hole-scavengers, the dosage of each COF is 2 mg.

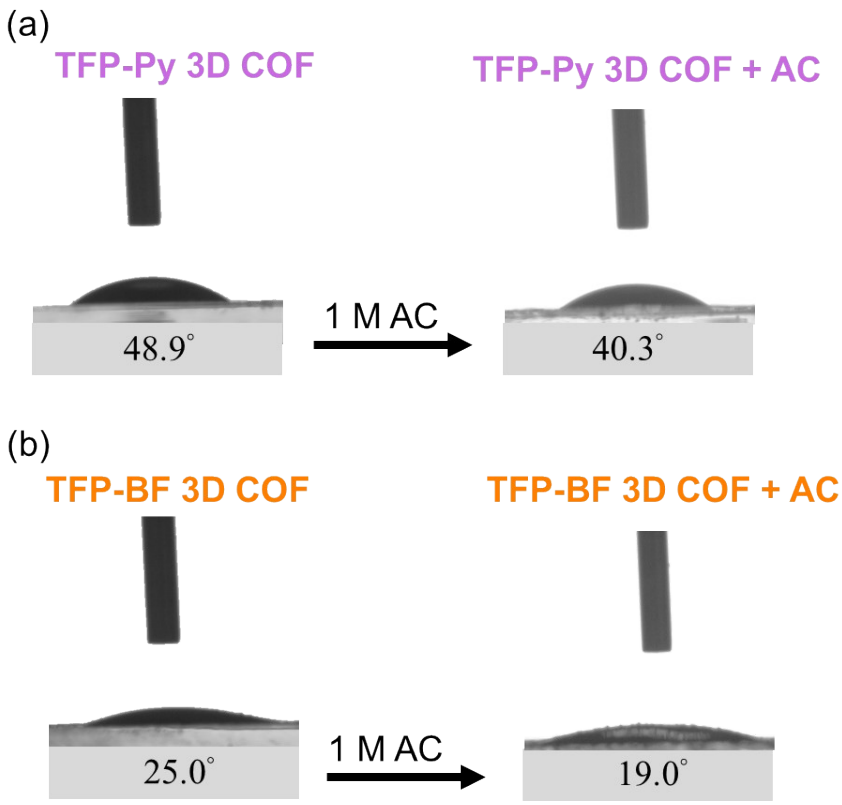

Figure S30. Water contact angles for (a) TFP-Py 3D COF before and after AC (1 M) treatment and (b) TFP-BF 3D COF before and after AC treatment.

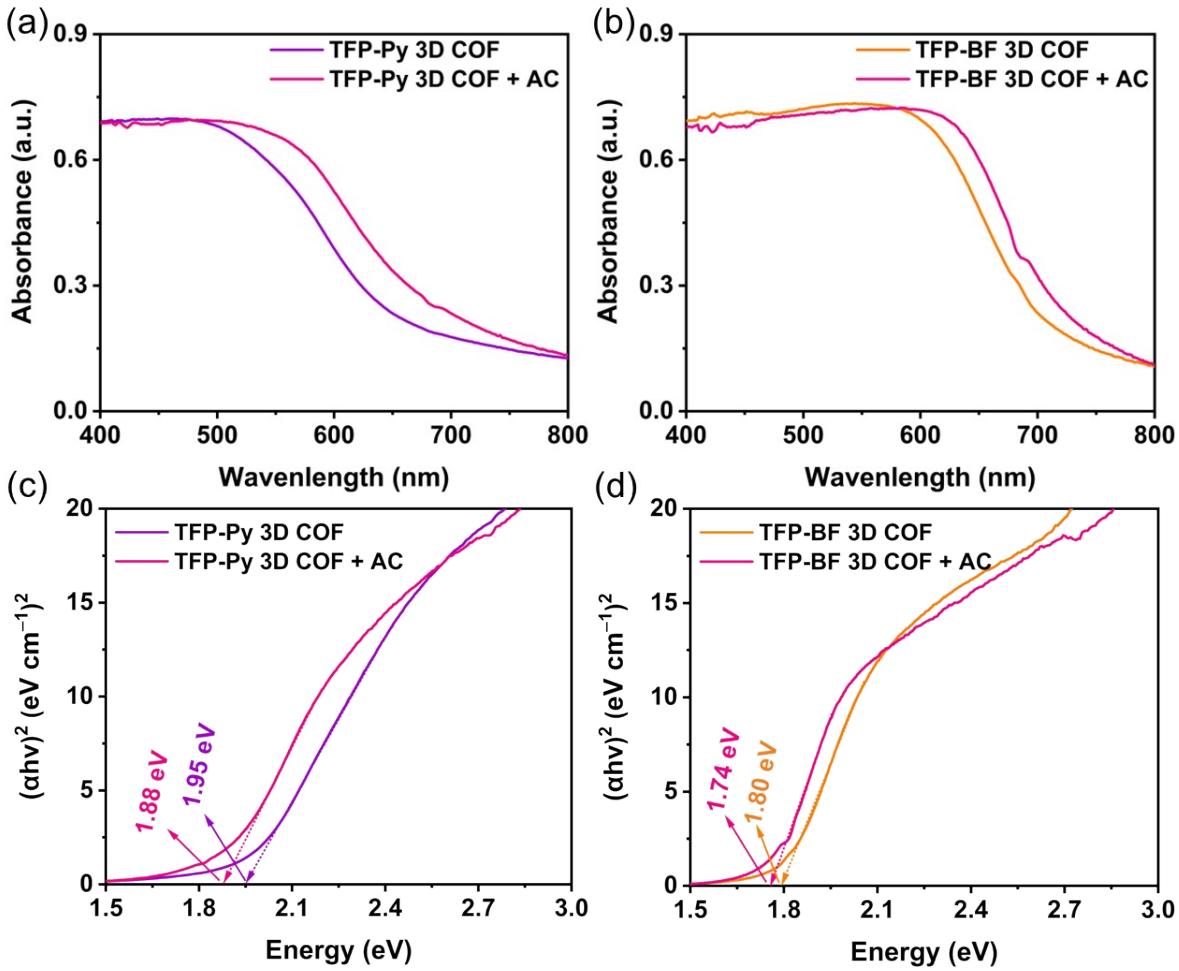

Figure S31. UV–Vis DRS spectra of (a) TFP-Py 3D COF before and after AC (1 M) treatment and (b) TFP-BF 3D COF before and after AC treatment. Tauc plots from the UV-Vis spectra of (c) TFP-Py 3D COF before and after AC (1 M) treatment and (d) TFP-BF 3D COF before and after AC treatment.

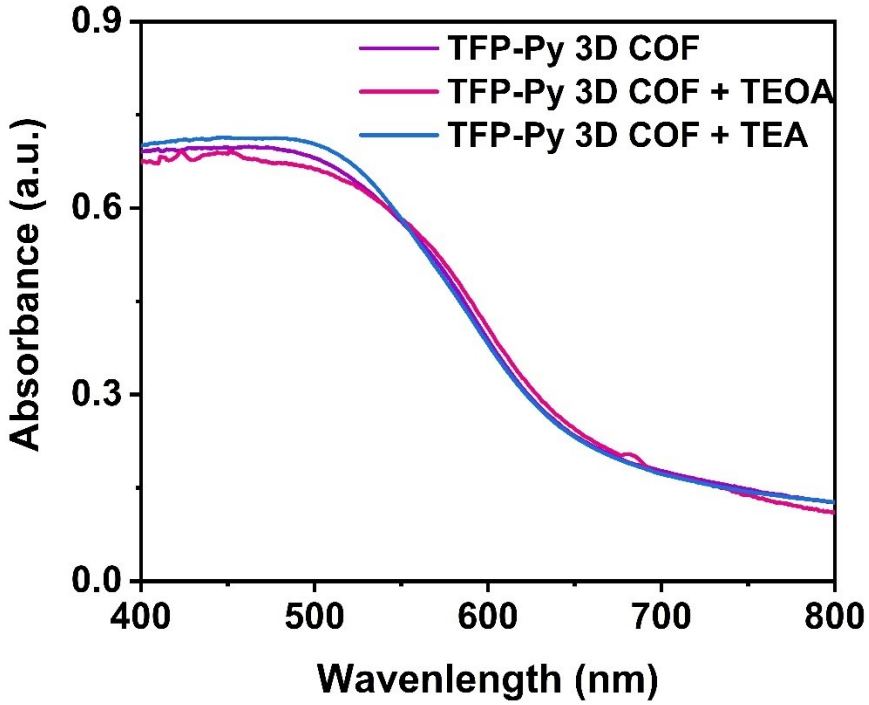

Figure S32. UV–Vis DRS spectra of TFP-Py 3D COF before and after treatment with 30%TEOA and 30%TEA aqueous solutions.

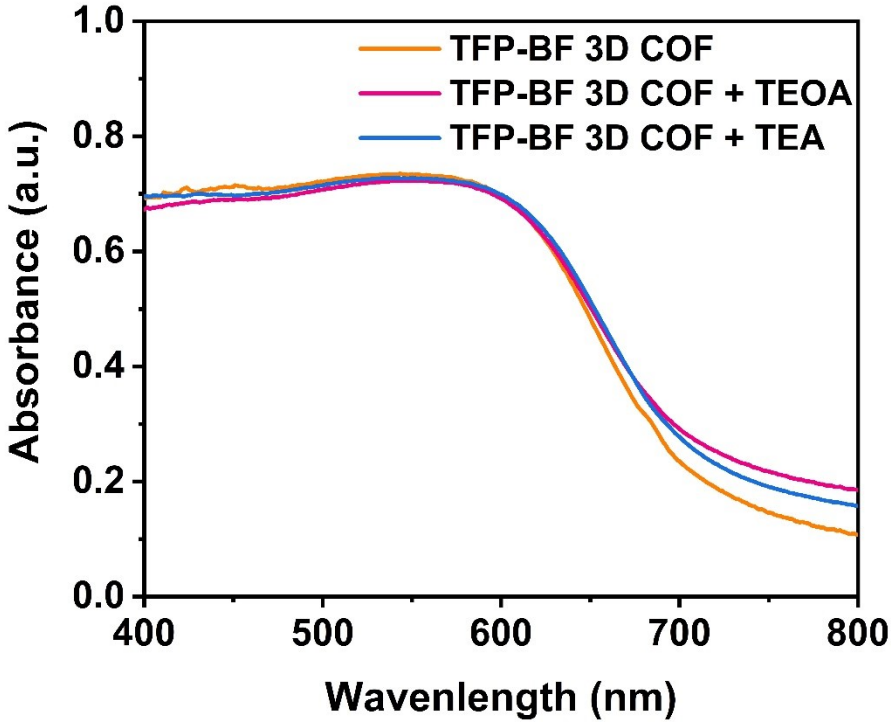

Figure S33. UV–Vis DRS spectra of TFP-BF 3D COF before and after treatment with 30%TEOA and 30%TEA aqueous solutions.

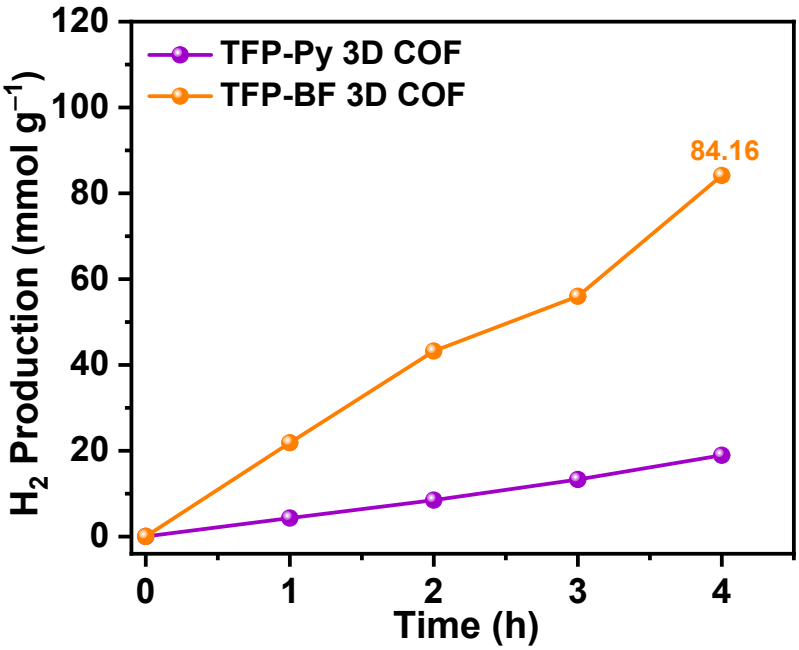

Figure 34. HERs of TFP-Py and TFP-BF 3D COFs using AA as the hole-scavenger under UV-Vis light, the dosage of each photocatalyst is 2 mg.

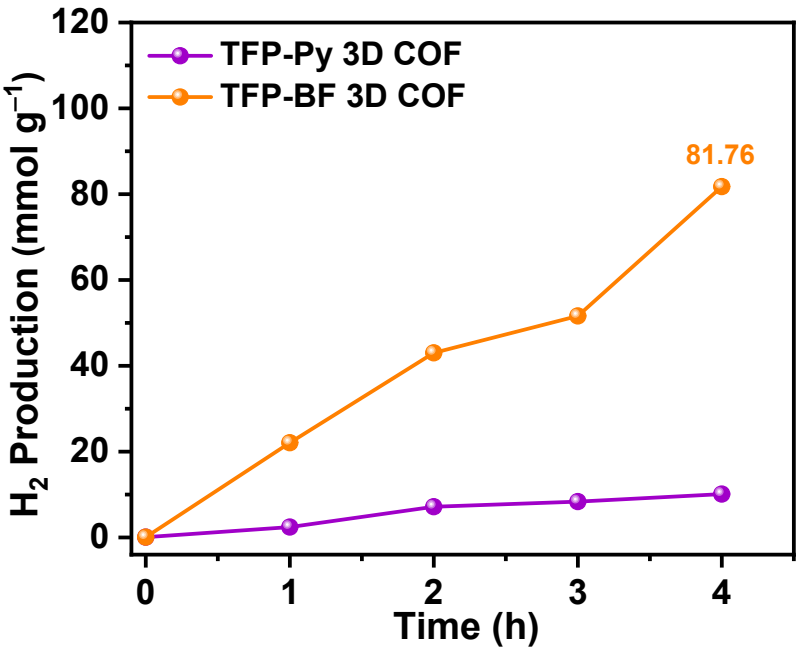

Figure 35. HERs of TFP-Py and TFP-BF 3D COFs using AA as the hole-scavenger under visible light, the dosage of each photocatalyst is 2 mg.

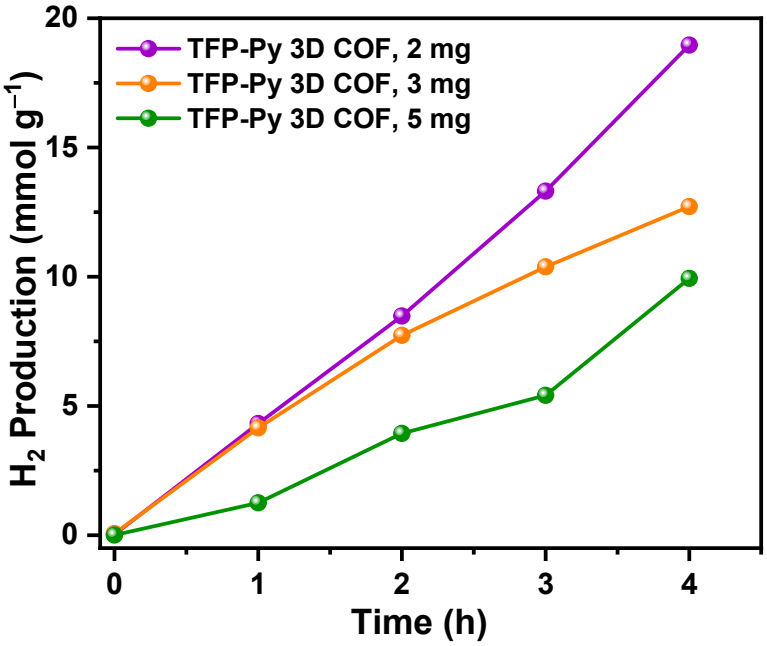

Figure S36. HERs of TFP-Py 3D COF using AA as the hole-scavenger under UV-Vis light, the dosage of each photocatalyst is different mass amounts.

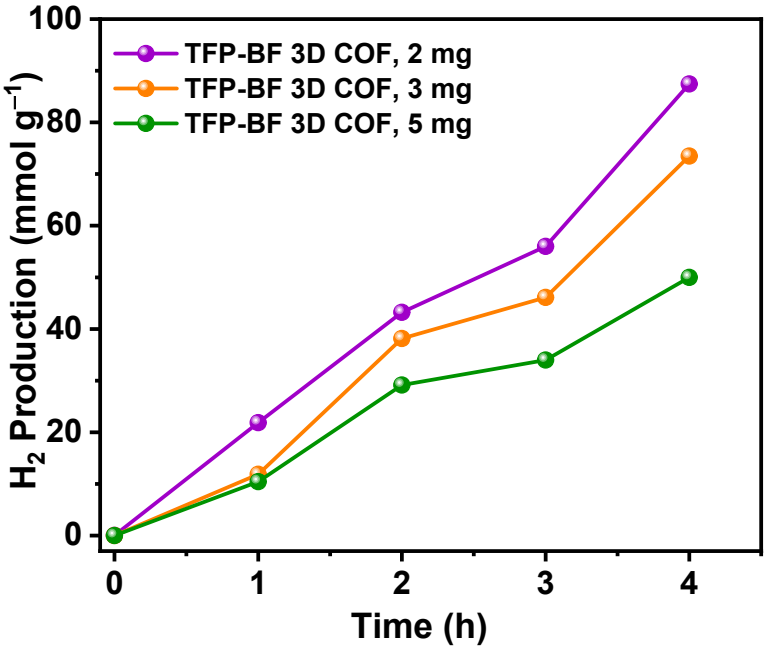

Figure S37. HERs of TFP-BF 3D COF using AA as the hole-scavenger under UV-Vis light, the dosage of each photocatalyst is different mass amounts.

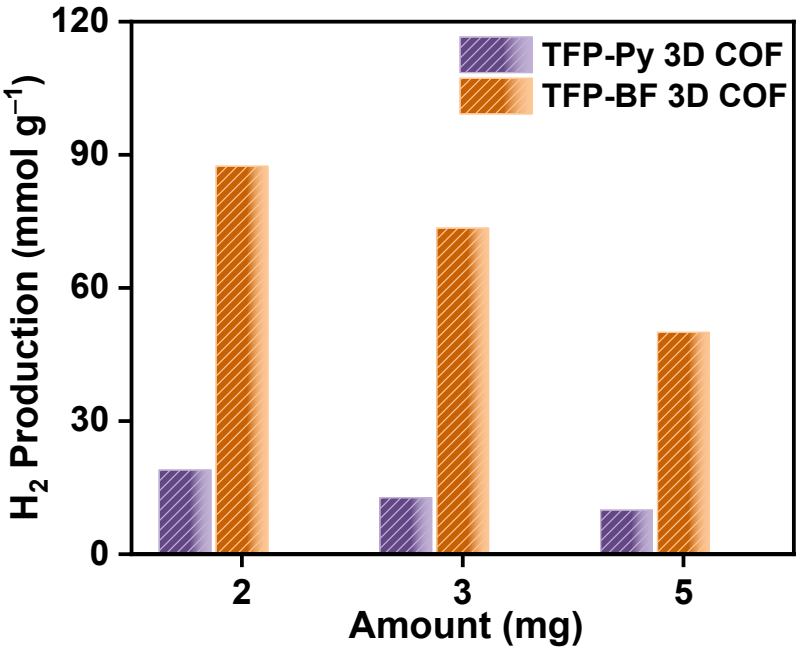

Figure 38. Comparison of HERs of TFP-Py and TFP-BF 3D COFs with different mass amounts under UV-Vis light.

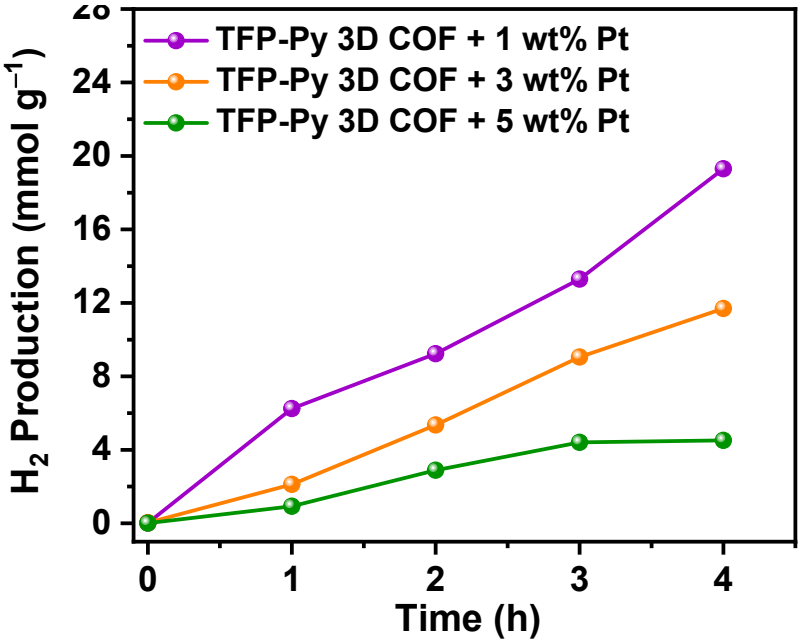

Figure 39. HERs of TFP-Py 3D COF with different concentrations of Pt co-catalyst , the dosage of each photocatalyst is 2 mg using AA as the hole-scavenger under UV-Vis light.

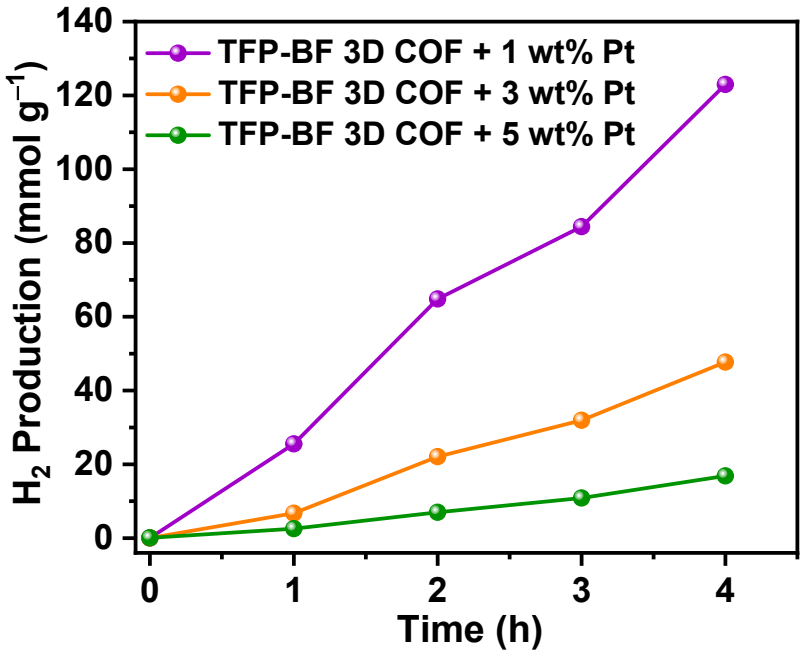

Figure 40. HERs of TFP-BF 3D COF with different concentrations of Pt co-catalyst , the dosage of each photocatalyst is 2 mg using AA as the hole-scavenger under UV-Vis light.

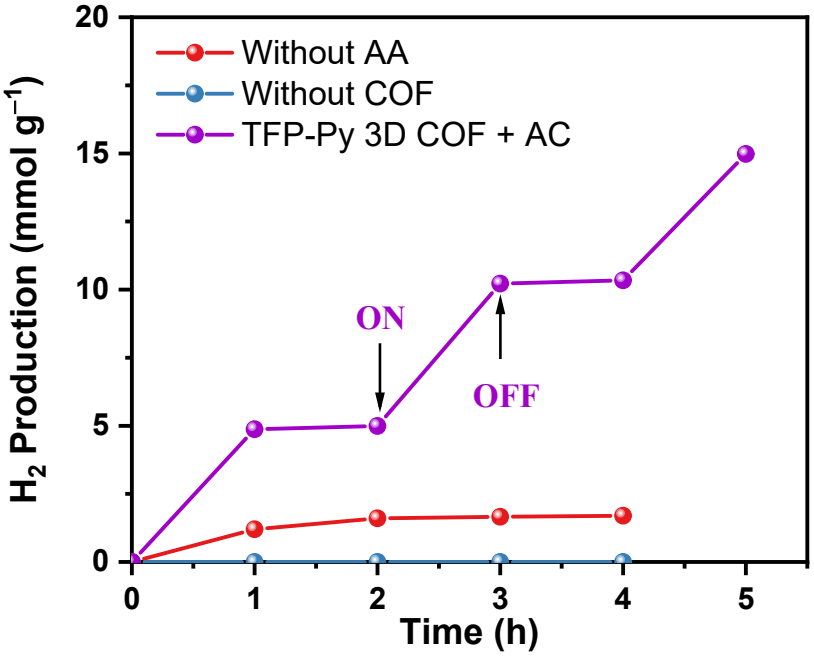

Figure 41. Control experiments of TFP-Py 3D COF, the dosage of each photocatalyst is 2 mg using AA as the hole-scavenger under UV-Vis light.

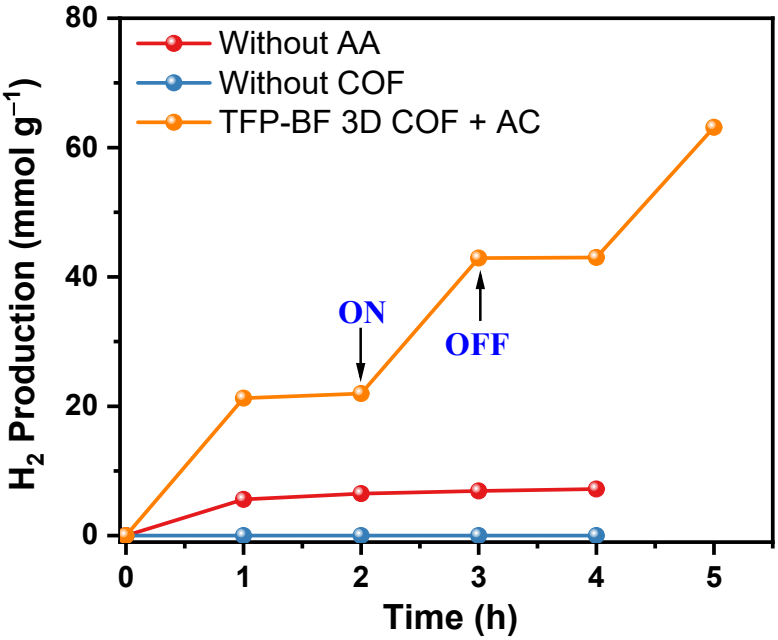

Figure 42. Control experiments of TFP-Py 3D COF, the dosage of each photocatalyst is 2 mg using AA as the hole-scavenger under UV-Vis light.

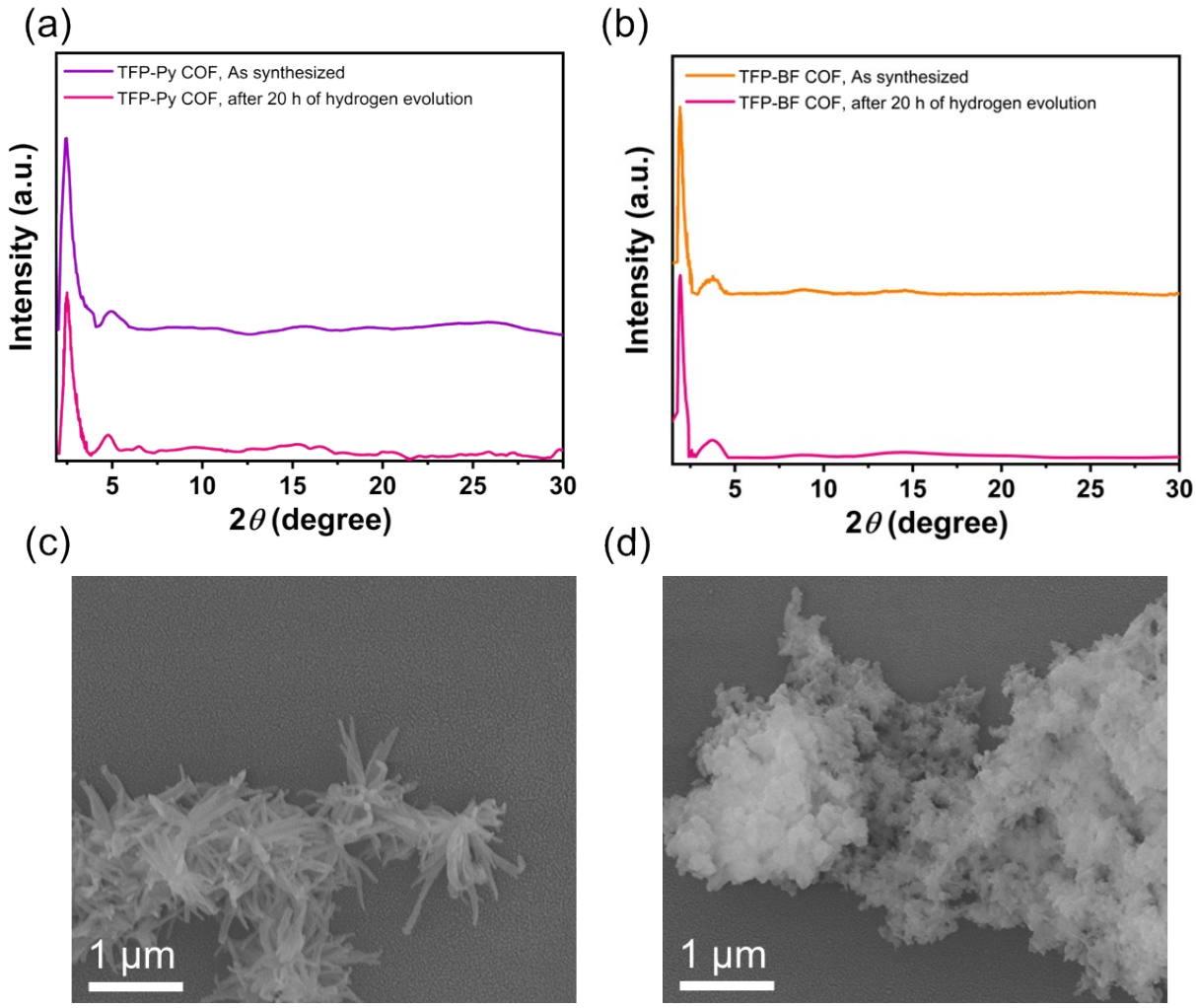

Figure S43. PXRD patterns of (a) TFP-Py and (b) TFP-BF 3D COFs before and after 4 cycles of the photocatalytic hydrogen evolution from water. FE-SEM images of (c) TFP-Py and (d) TFP-BF 3D COFs after 4 cycles of the photocatalytic hydrogen evolution from water.

Table S12. Comparative studies of synthesized COFs with the reported polymers toward photocatalytic hydrogen evolution.

Catalyst	Co-Catalyst	Catalyst amount (mg)	SED	HER ($mmol\ g^{-1}\ h^{-1}$)	Ref.
BT-COF	Pt (3.5 wt%)	10	AA	7.70	*Nat. Commun.* 2021, *12*, *3934*.
30%PEG@BTCOF	Pt (3.7 wt%)	10	AA	11.140	*Nat. Commun. 2021, 12, 3934*
Py-HTP-BT-COF	Pt (5wt%)	20	AA	1.078	*Angew. Chem. Int. Ed. 2020,59, 16902*
Py-ClTP-BTCOF	Pt (5wt%)	20	AA	8.875	*Angew. Chem. Int. Ed. 2020,59, 16902*
Py-FTP-BT-COF	Pt (5wt%)	20	AA	2.875	*Angew. Chem. Int. Ed. 2020,59, 16902*
PyTA-BC COF	Pt (7.4wt%)	1	AA	5.030	*Adv. Opt. Mater.* 2020, *8*, 2000641
S-COF	Pt (8wt%)	5	AA	4.44	*Nat. Chem. 2018, 10, 1180*
FS-COF	Pt (8wt%)	5	AA	10.100	*Nat. Chem. 2018, 10, 1180*
PyPz-COF	Pt (3.2wt%)	20	AA	7.542	*Small* 2023, 2207421.
BTT-NDA COF	Pt (3 wt%)	5	AA	5.22	*Angew.Chem. Int. Ed*. 2023, 62, e202217416
TAB-TFP-COF	Pt (3 wt%)	12.5	AA	0.666	*J. Mater. Chem. A, 2022,10, 17691-17698*
PyTz-COF	Pt (3 wt%)	35	AA	2.07	*Angew. Chem. Int. Ed.* 2021, *60*, 1869-1874
COF-BPDA	Pt (2.5 wt%)	20	AA	3.230	*J. Am. Chem. Soc. 2022, 144, 3653-3659*
BTT-BPy-PCCOF	Pt (3.32 wt%)	10	AA	12.3	*Angew. Chem. Int* 2023, 135, e202300224
Pt-PVP-TPCOF	Pt (6 wt%)	10	AA	8.420	*Angew. Chem. Int. Ed. 2019, 58, 18290*
g-C_3N_4/TTATP COF	Pt (2wt%)	100	TEOA	10.058	*Chem. Commun., 2019, 55, 5829*
SonoCOF-3	Pt (4wt%)	5	AA	16.600	*Nat. Synth. 2022, 1, 87*
BTH-3	Pt (8wt%)	5	AA	15.100	*Nat. Commun. 2022, 13, 100*
NKCOF-108	Pt (5wt%)	10	AA	11.600	*ACS Catal. 2021, 11, 2098*
TZ-COF-4	Pt (3.8wt%)	5	AA	4.296	*J. Am. Chem. Soc. 2020, 142, 11131*
COF–alkene	Pt (3wt%)	20	TEOA	2.330	*Adv. Sci. 2020, 7, 1902988*
TtaTfa COF	Pt (3.8wt%)	3	AA	2.330	*Angew. Chem., Int. Ed. 2021, 60, 19797-19803*
TpDTz COF	NiME	5	TEOA	0.941	*J. Am. Chem. Soc. 2019, 141, 11082*
sp^2C-COF_{ERDN}	Pt (3wt%)	50	TEOA	2.210	*Chem 2019, 5, 1632*

g-$C_{18}N_3$-COF	Pt (3wt%)	50	AA	0.292	*J. Am. Chem. Soc. 2019, 141, 14272*
g-$C_{40}N_3$-COF	Pt (3wt%)	50	TEOA	2.596	*Nat. Commun. 2019, 10, 2467*
TP-BDDA COF	Pt (3wt%)	10	TEOA	0.324	*J. Am. Chem. Soc. 2018, 140, 1423*
N_3-COF	Pt (0.68wt%)	5	TEOA	1.730	*Nat. Commun. 2015, 6, 8508*
TFPT-COF	Pt (2.2wt%)	10	TEOA	1.970	*Chem. Sci., 2014, 5, 2789*
ZnPor-DETH-COF	Pt (8wt%)		TEOA	0.413	*Nat. Commun. 2021, 12, 1354*
TFP-Py COF	Non	2	AA	4.96	**This work**
TFP-BF COF	Non	2	AA	21.04	**This work**
TFP-TPT COF	Non	2	AA	2.68	**This work**

DFT calculations

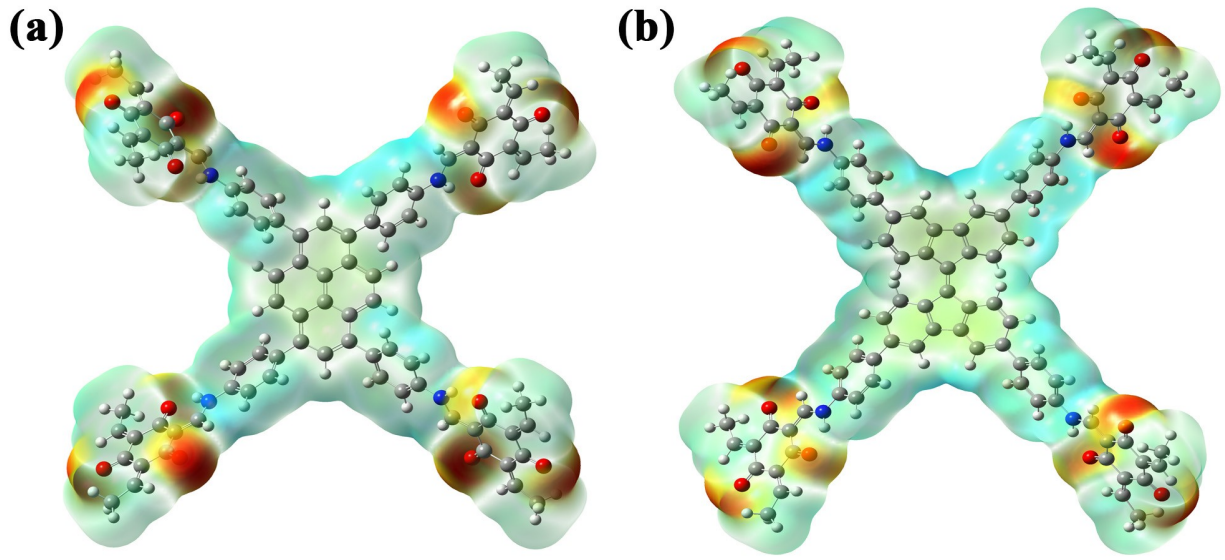

Fig. S44. Electrostatic potential (ESP) distributions of (a) TFP-Py and (b) TFP-BF COFs.

Table S13. The calculated MOs energies, energy gap, and global reactivity parameters of the studied molecules.

Quantum descriptors	TFP-Py COF	TFP-BF COF
E_{HOMO} (eV)	-4.83	-4.84
E_{LUMO} (eV)	-3.27	-3.56
ΔE (eV)	1.56	1.28
Electron affinity A (eV)	3.27	3.56
Ionization potential I (eV)	4.83	4.84
Chemical hardness η (eV)	0.78	0.64
Softness S (eV^{-1})	0.64	0.78
Electronegativity χ (eV)	4.05	4.20
Electrophilicity index ω (eV)	10.52	13.79
Chemical potential μ (eV)	-4.05	-4.20

Table S14. Fukui index of RhB dye calculated by DFT.

Atom Site	Mulliken Charge	Electrophilic Attack (f^-)	Nucleophilic Attack (f^+)	Radical Attack (f^0)
O(1)	-0.494	0.013	0.029	0.021
O(2)	-0.450	0.013	0.016	0.015
O(3)	-0.414	-0.003	0.000	-0.001
N(4)	-0.304	0.061	0.039	0.050
N(5)	-0.303	0.063	0.039	0.051
C(6)	0.023	0.022	0.076	0.049
C(7)	0.050	0.034	0.017	0.025
C(8)	0.061	0.035	0.017	0.026
C(9)	0.326	0.013	0.021	0.017
C(10)	0.327	0.013	0.021	0.017
C(11)	0.229	0.020	0.032	0.026
C(12)	0.230	0.020	0.032	0.026
C(13)	0.048	-0.012	-0.011	-0.012
C(14)	-0.167	0.029	0.021	0.025
C(15)	-0.169	0.031	0.021	0.026
C(16)	-0.116	0.024	0.035	0.030
C(17)	-0.106	0.024	0.035	0.030
C(18)	-0.109	0.035	0.035	0.035
C(19)	-0.110	0.035	0.035	0.035
C(20)	-0.010	0.010	0.007	0.009
C(21)	-0.007	0.011	0.007	0.009
C(22)	-0.008	0.011	0.007	0.009
C(23)	-0.010	0.011	0.008	0.009
C(24)	0.014	0.000	0.003	0.002
C(25)	-0.056	0.000	0.004	0.002
C(26)	-0.154	0.013	0.009	0.011
C(27)	-0.154	0.013	0.009	0.011
C(28)	-0.154	0.013	0.009	0.011
C(29)	-0.154	0.013	0.009	0.011
C(30)	-0.050	0.012	0.015	0.014
C(31)	-0.031	0.012	0.016	0.014
C(32)	-0.043	0.017	0.021	0.019
C(33)	0.486	0.001	0.001	0.001

Table S15. Gibbs free energy changes (ΔG) of hydrogen adsorption on different active sites.

Samples	Site 1 (Oxygen atom)	Site 2 (Nitrogen atom)
TFP-Py COF	0.39 eV	2.15 eV
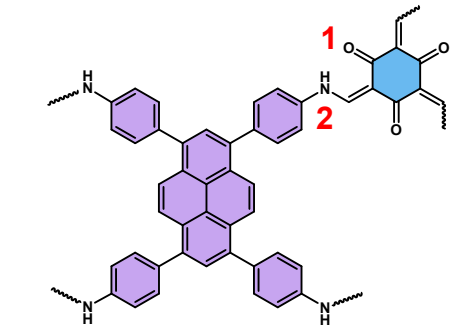		
TFP-BF COF	0.36 eV	2.10 eV
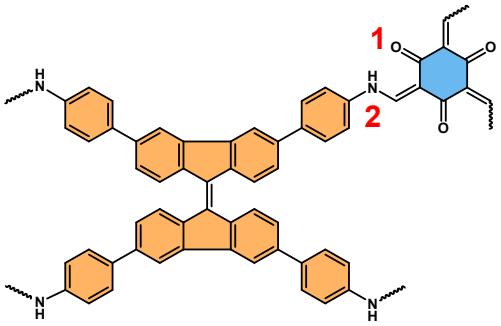		

Reference:

S1. C. Yang, Z. Cheng, G. Divitini, C. Qian, B. Hou, Y. Liao, *J. Mater. Chem. A,* 2021, **9**, 19894–19900.

S2. Sivakarthik, V. Thangara, M. Parthibavarman, *J. Mater. Sci.: Mater. Electron.,* 2017, **28**, 5990–5996.

S3. Riken Keiki Co., Tokyo, model AC-3, http://www.rikenkeiki. co.jp/english/.

S4. Y. Guo, W. Sato, K. Inoue, W. Zhang, G, Yu, E. Nakamura, *J. Mater. Chem. A,* 2016, **4**, 18852–18856.

S5. M. Onoda, K.Tada, H. Nakayama, *J. Appl. Phys.,* 1999, **86**, 2110.

S6. J. Jasieniak, M. Califano, S. E. Watkins, *ACS Nano*, 2011, **5**, 5888–5920.

S7. T. Kameyama, T. Takahashi, T. Machida, Y. Kamiya, T. Yamamoto, S. Kuwabata, T. Torimoto, *J. Phys. Chem. C, 2015*, **119**, 24740–24749.

S8. S. Lacher, Y. Matsuo, E. Nakamura, *J. Am. Chem. Soc.,* 2011, **133**, 16997–17004.

S9. Zakaria, M. B. Belik, A. A. Liu, C. H. Hsieh, H. Y. Liao, Y. T. Malgras, V. Yamauchi, Y. Wu, K. C. W. *Chem. Asian J.* **2015**, *10*, 1457–1462.